Dynamical Climatology

Parameter regimes for studying isolated eddies.

by

P.D. Killworth and M.K. Davey

DCTN 42

June 1986

Meteorological Office (Met. O. 20)
London Road
Bracknell
Berkshire RG12 2SZ

DYNAMICAL CLIMATOLOGY TECHNICAL NOTE NO. 42

PARAMETER REGIMES FOR STUDYING ISOLATED EDDIES

by

P D Killworth

Institute of Oceanographic Sciences,
Wormley, Godalming, Surrey.

and

M K Davey

Meteorological Office, Hooke Institute, Oxford

Met O 20 (Dynamical
Climatology Branch)
Meteorological Office
London Road
Bracknell
Berkshire, U.K. RG12 2SZ

June 1986

Note: This paper has not been published. Permission to quote from it should be obtained from the Assistant Director of the above Meteorological Office branch.

PARAMETER REGIMES FOR STUDYING ISOLATED EDDIES

Peter D. Killworth [1] and Michael K. Davey [2]

Hooke Institute for Atmospheric Research

Clarendon Laboratory

Parks Road

Oxford OX1 3PU

and

[1] Institute of Oceanographic Sciences

Wormley

Godalming

Surrey

and

[2] Meteorological Office

Bracknell

Berkshire

ABSTRACT

The parameter ranges relevant to propagating oceanic eddies are explored with a view to simplifying the equation sets previously used to simulate such eddies. The reduced gravity shallow-water model is used as a starting point. We consider eddies whose width is of the same order as, or somewhat larger than, the Rossby deformation radius. Two model equations emerge from these scalings, both permitting modon solutions and easy numerical integration. Both, too, give fair simulations of the shallow-water model, but disagree in details.

Using another approach, an ad hoc vortex model is used to predict the path of an eddy. This also gives a fair but not perfect simulation of the one-layer results. It appears that the only ideal way to reproduce primitive equation results accurately is to use the primitive equations themselves.

1. INTRODUCTION

The properties of isolated oceanic eddies have been intensively studied in the past decade, both observationally (McDowell and Rossby, 1978; Dugan et al., 1982) and theoretically (McWilliams and Flierl, 1979; Shen, 1981). Most of the theoretical studies have, for reasons of analytical tractability, concentrated upon steady propagating eddies, usually in a quasigeostrophic framework. Those studies that examined eddies which were not steadily propagating (or nearly so; Nof, 1984) have been exclusively numerical, employing either quasigeostrophy or one- or two-layer primitive equations (McWilliams and Flierl, 1979; Mied and Lindemann, 1979).

It seemed to us that there was a need for some middle ground. Could an equation set simpler than the primitive equations be produced which would both yield insight as to the operant physics and also improve the numerical integration times?

Such equations have already been discussed by Matsuura and Yamagata (1982) and Gent and McWilliams (1983). The latter conclude that some form of the balance equations is necessary for high accuracy in integration (which could not speed up the calculations) but that either quasigeostrophy or the "active scalar" equation (depending on the ratio of length scale to Rossby radius) make an acceptable approximation to leading order. Both are easily integrated numerically.

In this paper we re-examine the parameter ranges relevant to some

oceanic eddies. It turns out that for either a single layer fluid, or for a single vertical normal mode in a continuous fluid (a case mentioned by Gent and McWilliams, 1984), another balance is possible, not noted by the above authors' surveys, applying to eddies with horizontal scales wider than a deformation radius. The resulting equation is easy to integrate numerically. Results are compared with those of the shallow-water model of Davey and Killworth (1984) henceforth referred to as D & K.

A second approach consists of an ad hoc model of an eddy as a circular vortex. A simple set of equations for the propagation of the eddy centre is derived, which allows rapid qualitative prediction of eddy evolution.

2. NON-DIMENSIONAL EQUATIONS AND PARAMETERS

We start with continuously stratified equations using density as a vertical co-ordinate. With some alterations noted below these also represent the shallow-water (one layer reduced gravity) equations, which also govern an intrusive layer sandwiched between much deeper layers. Axes have x east and y north, with velocity components u and v respectively. Motion is on a beta-plane, so the Coriolis parameter is

$$f = f_0 + \beta y$$

The dimensional equations are:

$$u_t + \underline{u}.\nabla u - fv = - B_x \qquad (2.1)$$

$$v_t + \underline{u}.\nabla v + fu = - B_y \qquad (2.2)$$

$$h_t + \nabla.(h\underline{u}) = 0 \qquad (2.3)$$

with either

$$B = g'h \qquad \text{(shallow-water)} \qquad (2.4)$$

or

$$B_\rho = gz/\rho_0$$

(continuous stratification) (2.5)

$$h = \rho_0 z_\rho$$

Here B is the linear Bernouilli function, g' is a reduced gravity, and h is the layer depth in the shallow-water case. In the continuously stratified case z is the depth of density ρ, and ρ_0 is a characteristic density. Undisturbed depth of fluid is H, and N_0 is a measure of the buoyancy frequency, such that the gravity wave speed is

$$c = \begin{cases} N_0 H & \text{(continuous)} \\ (g'H)^{1/2} & \text{(shallow-water)} \end{cases} \qquad (2.6)$$

D & K took the "natural" non-dimensional form, using c as a velocity scale, f_0 as time scale, and Rossby radius $R = c/f_0$ as length scale. This yielded a single dimensionless parameter $\beta R/f_0$ (Gent & McWilliams 1983 call this R_β), which is equivalent to the ratio $\hat{c}/c$ where

$$c = \beta R^2 \qquad (2.7)$$

is the speed of a long Rossby wave. This ratio is small in practice because f does not change much within an eddy. The experiments described in D & K did not totally fit such scaling: the eddy length scale L was several Rossby radii with maximum flow speed U much smaller than c, so the Rossby number

$$Ro = U/f_0 L \qquad (2.8)$$

was small. The time scale for eddy evolution was not f_o^{-1} but a much longer scale, like the scale $L/\hat{c}$ for long Rossby waves. Matsuura & Yamagata (1982) used such features to obtain simplified equations relevant to large eddies observed in the Pacific, and we shall follow and extend their approach here.

Thus we use length scale L, time scale $L/\hat{c}$ and velocity scale U. For the shallow-water version we define a non-dimensional scaled surface displacement η^* by

$$h = H\,[\,1 + (UL/cR)\eta^*\,] \tag{2.9}$$

For the continuously stratified case we put

$$z = H\,[\,z_o^*(\rho^*) + (UL/cR)z^*\,] \tag{2.10}$$

$$\rho = \rho_o N_o^2 H\rho^*/g \tag{2.11}$$

$$B = c^2\,[\,\int z_o^* d\rho^* + (UL/cR)B^*\,] \tag{2.12}$$

$$h = (g/N_o^2)\,[\,dz_o^*/d\rho^* + (UL/cR)\eta^*\,] \tag{2.13}$$

where $z_o^*(\rho^*)$ is a non-dimensional measure of the static stratification. Thus z^* indicates the perturbation in the depth of a density value and η^* is a measure of "thickness" change. The scalings (2.10) - (2.13) are not independent, for we have from (2.5)

$$z^* = \partial B^*/\partial \rho^* \tag{2.14}$$

$$\eta^* = \partial z^*/\partial \rho^* = \partial^2 B^*/\partial \rho^{*2} \tag{2.15}$$

Dropping the asterisks, (2.1) - (2.3) take the non-dimensional form

$$\epsilon F^{-1} u_t + Ro\ \underline{u}.\nabla u - (1 + \epsilon y)\ v = - B_x \tag{2.16}$$

$$\epsilon F^{-1} v_t + Ro\ \underline{u}.\nabla v + (1 + \epsilon y)\ u = - B_y \tag{2.17}$$

$$\epsilon \eta_t + (dz_0/d\rho)\nabla.\underline{u} + F\ Ro\ \nabla.(\underline{u}\eta) = 0 \tag{2.18}$$

with either

$$B = \eta$$

$$\text{(shallow-water)} \tag{2.19}$$

$$dz_0/d\rho = 1$$

or

$$B_{\rho\rho} = \eta \quad \text{(continuously stratified).} \tag{2.20}$$

The two new non-dimensional parameters are

$$\epsilon = \beta L/f_0 \tag{2.21}$$

$$F = L^2/R^2 \tag{2.22}$$

The Froude number F is (eddy scale/Rossby radius)^2. Note that

$$F\,Ro = (UL/cR). \tag{2.23}$$

In non-dimensional form, potential vorticity is

$$q = \frac{Ro\,(v_x - u_y) + 1 + \epsilon y}{dz_0/d\rho + F\,Ro\,\eta} \tag{2.24}$$

This is a conserved quantity for each fluid element:

$$\epsilon F^{-1} q_t + Ro\,\underline{u}.\nabla q = 0 \quad . \tag{2.25}$$

Typical midlatitude scales, as used in D&K, are

$$\beta = 2\times10^{-11} m^{-1}s^{-1},\ f = 7.3\times10^{-5} s^{-1},\ c^2 = 9.8\ m^2 s^{-2} \tag{2.26}$$

giving a deformation radius R of 43 km. The quantities U and L may vary from case to case. We note, though, that even for L as large as 200 km, we have $\epsilon < 0.05$, so we can safely assume

$$\epsilon << 1 \tag{2.27}$$

For the cyclonic eddy experiments C3 and C4 of D&K - a mildly nonlinear eddy and a substantially nonlinear eddy respectively - relevant values of

U based on maximum speeds were 0.05 m s^{-1} and 0.55 m s^{-1}, giving

$$Ro = \begin{cases} 0.008 & (C3) \\ 0.09 & (C4) \end{cases} \qquad (2.28)$$

In both cases L was about 2 R, so $F \approx 4$ and $\epsilon \approx 0.024$. These values may be taken as typical, bracketing many of the observed values for oceanic lenses (cf. Dugan et al., 1982). In the analysis to follow

$$Ro \ll 1 \qquad (2.29)$$

will be assumed. The value of F is more difficult to interpret: is 4 large compared with, or of the same magnitude as, 1? The case of F of order unity gives quasigeostrophy, so we will mainly consider F large, of order $\epsilon^{-1/2}$. For comparison, Matsuura and Yamagata (1982) chose $Ro \approx \epsilon^2$, $F \approx \epsilon^{-1}$; Gent and McWilliams (1983) examined the cases Ro $\ll$, $\approx$, $\gg \epsilon$; $F \lesssim \epsilon$, ≈ 1, $\gg \epsilon^{-1}$.

In this notation, the measure of nonlinearity $U/\hat{c}$ used by D&K is $F\,Ro/\epsilon$, taking the values 1.4 for C3 and 15 for C4.

3. EDDIES MUCH WIDER THAN A DEFORMATION RADIUS: $F = \mu\epsilon^{-1/2}$, $\mu = O(1)$

If we first consider F to be of order unity, then expansions of the equations in Section 2 in powers of ϵ, for $Ro = O(\epsilon)$, merely generate the familiar quasigeostrophic equations (henceforth QG). For a one-layer fluid, for example, one obtains dimensionally

$$\{\partial/\partial t + J(\Psi, \ ) \} [\nabla^2\Psi - R^{-2}\Psi + \beta y] = 0 \qquad (3.1)$$

where Ψ is a streamfunction defined by

$$\Psi = g'Hf_o^{-1}FRo\ h \qquad (3.2)$$

and $J(a,b) = a_x b_y - a_y b_x$ is the horizontal Jacobian. The QG equation is unaffected by the transformation Ψ <--> $-\Psi$, y <--> $-y$, so that the westward propagation of cyclones with $\Psi < 0$ and anticyclones with $\Psi > 0$ behave the same, since the fluid depth in either case is constant to leading order. Integrations of (3.1) along the lines of the Ball (1963) calculation (cf. Killworth 1983 for details) show that the centres of both mass and potential vorticity move westward at the long Rossby wave speed.

If, however, F is larger than unity then other physical effects come into play. Gent and McWilliams (1983) derive the active scalar equation for F of order ϵ^{-1}, but the eddies studied by D&K are not that wide. It turns out that under certain circumstances another equation, omitted by

both Williams and Yamagata (1984) and Gent and McWilliams (1983) can hold, if F is $O(\epsilon^{-1/2})$, as will now be shown. The derivation uses a continuously stratified fluid; modifications for a one-layer fluid are noted where necessary.

(a) $Ro = \alpha\epsilon$, $\alpha = O(1)$

The first possibility we consider is that $Ro = O(\epsilon)$. We expand quantities in powers of $\epsilon^{1/2}$, e.g.

$$B = B^0 + \epsilon^{1/2}B^1 + \epsilon B^2 + \ldots$$

and substitute into eqns. (2.16) to (2.18). To leading order the motion is geostrophic:

$$v^0 = B^0_x \tag{3.3}$$

$$u^0 = -B^0_y \tag{3.4}$$

$$u^0_x + v^0_y = 0. \tag{3.5}$$

At $O(\epsilon^{1/2})$, geostrophy remains but mass continuity differs:

$$v^1 = B^1_x \tag{3.6}$$

$$u^1 = -B^1_y \tag{3.7}$$

$$(u^0h^0)_x+(v^0h^0)_y = 0. \qquad (3.8)$$

To satisfy the (3.8) (which occurs automatically for a single layer fluid), we need

$$h^0 = B^0_{\rho\rho} = \text{function}\ (\rho, B^0).$$

We <u>choose</u> here a vertical normal mode such that

$$B^0 dz_0/d\rho = \gamma B^0_{\rho\rho}\ , \text{ with } B^0 = 0 \qquad \text{at top, bottom} \qquad (3.9)$$

for some "speed" γ relevant for the mode under consideration (cf. the comments in Gent and McWilliams, 1984).

Then, to $O(\epsilon)$, we have

$$\alpha(u^0u^0_x + v^0u^0_y) - v^2 - yv^0 + B^2_x = 0 \qquad (3.10)$$

$$\alpha(u^0v^0_x + v^0v^0_y) + u^2 + yu^2 + B^2_y = 0 \qquad (3.11)$$

$$h^0 + (dz_0/d\rho)(u^2_x+v^2_y) + \alpha\mu\{(h^0u^1+h^1u^0)_x + (h^0v^1+h^1v^0)_y\} = 0. \qquad (3.12)$$

The last parenthesis { } in (3.12) vanishes if the normal mode holds to $O(\epsilon^{1/2})$, so that

$$B^1 dz_0/d\rho = \gamma B^1_{\rho\rho} \quad \text{also.} \qquad (3.13)$$

Algebra then gives

$$\gamma^{-1} B^0_t = B^0_x + \alpha \underline{u}^0 . \nabla \zeta^0 \qquad (3.14)$$

where $\zeta = v_x - u_y$ is the relative vorticity. This equation represents the movement of long nonlinear Rossby waves. They are long because the eddies are wide. The balance $\gamma^{-1} B^0_t \approx B^0_x$ would represent westward motion at the nondimensional long Rossby wave speed $-\gamma$. (γ is unity for a single layer of fluid.) They are nonlinear because the Rossby number is sufficiently large to modify vorticity on the same scale as variations in f.

A radially symmetric travelling solution to (3.14) may be written as

$$B^0 = B^0(r), \text{ where } r=[(x + \gamma t)^2 + y^2]^{1/2}. \qquad (3.15)$$

The radial symmetry ensures no advection of vorticity by the geostrophic flow. Thus in this regime an initially symmetric eddy will simply propagate westwards bodily at the long wave speed with no change in shape.

(b) Less nonlinear: $Ro = \alpha\epsilon^{3/2}$, $\alpha = O(1)$

The ratio $U/\hat{c}$ is formally reduced as nonlinearity is reduced. The parameter range $Ro = O(\epsilon^{3/2})$ gives $U/\hat{c} = O(1)$, which should be a reasonable fit to D&K's C3, and possibly to the C4, experiments. (α = 2.2 for C3, and 24 for C4.)

It will be convenient to introduce a slow time $T = \epsilon^{1/2}t$ with dimensional scale $\epsilon^{-1/2}L/\hat{c}$. This is about 190 days for our typical scales, compared with the normal time scale of about 1 month. Both timescales now enter the problem. Thus (2.16) to (2.18) become, neglecting terms of higher order than $\epsilon^{3/2}$,

$$\mu^{-1}\epsilon^{3/2}u_t + \alpha\epsilon^{3/2}(uu_x+vu_y) - (1+\epsilon y)v + B_x = 0. \qquad (3.16)$$

$$\mu^{-1}\epsilon^{3/2}v_t + \alpha\epsilon^{3/2}(uv_x+vv_y) + (1+\epsilon y)u + B_y = 0. \qquad (3.17)$$

$$\epsilon h_t + \epsilon^{3/2}h_T + (dz_e/d\rho)(u_x+v_y) + \alpha\mu\epsilon[(hu)_x+(hv)_y] = 0. \qquad (3.18)$$

We expand in powers of $\epsilon^{1/2}$. The O(1) terms are as in (3.7); order $\epsilon^{1/2}$ terms as (3.8) but with the last equation replaced by the identity $u^1_x + v^1_y = 0$. To $O(\epsilon)$ we find, after some cancellation, the system

$$-v^2 - yv^0 + B^2_x = 0 \qquad (3.19)$$

$$u^2 + yu^0 + B^2_y = 0 \qquad (3.20)$$

$$h^0_t + (dz_e/d\rho)(u^2_x + v^2_y) + \alpha\mu[(u^0h^0)_x + (v^0h^0)_y] = 0. \qquad (3.21)$$

Elimination gives a version of the "β active scalar equation" (Gent and McWilliams, 1983):

$$h^0_t - (dz_0/d\rho)B^0_x + \alpha\mu J(B^0,h^0) = 0; \tag{3.22}$$

note that the last term vanishes identically for a single layer fluid. Although (3.22) is applicable as it stands, we choose here to make the last term vanish by again seeking a single vertical normal mode (3.9). Thus (3.22) becomes merely

$$B^0_t = \gamma B^0_x \tag{3.23}$$

and

$$B^0 = B^0(X,y,T) \tag{3.24}$$

where

$$X = x + \gamma t \tag{3.25}$$

is an axis moving west at the long Rossby wave speed. Patterns thus travel westwards at speed γ and are modified on the longer time scale T.

To $O(\epsilon^{3/2})$, we obtain

$$\mu^{-1}u^0_t + \alpha(u^0u^0_x+v^0u^0_y) - v^3 - yv^1 + B^3_x = 0. \tag{3.26}$$

$$\mu^{-1}v^0_t + \alpha(u^0v^0_x+v^0v^0_y) + u^3 + yu^1 + B^3_y = 0. \tag{3.27}$$

$$h^0_\tau + h^1_t + (dz_o/d\rho)(u^3_x + v^3_y) + \alpha\mu[J(B^0,h^1)+J(B^1,h^0)] = 0. \qquad (3.28)$$

Elimination of u^3, v^3, and B^3 gives

$$h^1_t - (dz_o/d\rho)B^1_x = (dz_o/d\rho)\{\mu^{-1}\zeta^0_t + \alpha\underline{u}^0.\nabla\zeta^0\} - h^0_\tau. \qquad (3.29)$$

We assume again that the single normal mode structure holds to $O(\epsilon^{1/2})$, so that the Jacobians vanish (again, they automatically vanish for a single fluid layer). To avoid secularity on the LHS of (3.29) the RHS must vanish, giving finally, after use of (3.25) to replace t derivatives by X derivatives times γ,

$$B^0_\tau = \mu^{-1}\gamma^2\nabla^2B^0_X + \alpha\gamma J(B^0,\nabla^2B^0) \qquad (3.30)$$

where the Laplacian and Jacobian now refer to the moving frame (X,y). The structure of (3.30) is reminiscent of the Korteweg-de-Vries equation. It contains a third-order dispersion term $\nabla^2B^0_X$ as well as a nonlinear advection term. Such combinations frequently enter when one or both length scales are in some sense long; cf. Redekopp (1977).

Returning to dimensional terms, we have (for a single layer)

$$\Psi_t = \beta R^4\nabla^2\Psi_x + R^2J(\Psi,\nabla^2\Psi) \qquad (3.31)$$

where the Laplacian refers to a coordinate system moving due west at speed βR^2. The dispersive term can be recognised as the second term in the

long wave expansion of the linear Rossby wave equation. For waves varying as exp i(kx + ly - ωt),

$$\omega = -\beta k/(k^2 + l^2 + R^{-2}) \approx -\beta k R^2 + \beta k(k^2+l^2)R^4 \qquad (3.32)$$

Equation (3.31) will henceforth be referred to as the DA (dispersal advection) equation.

It is easy to show that the centres of mass and potential vorticity move westwards at speed $\hat{c}$ (as, indeed, they must if FRo << 1, as the depth is constant to leading order).

Solutions to (3.31) of soliton (modon) form may be sought. The method is familiar (e.g. Flierl et al., 1980) and is not repeated here. Because of the form of the first term on the RHS of (3.31), solitons with zero mass deficit move <u>westwards</u> relative to the long wave speed, unlike the isolated eddies of the previous paragraph.

Again, the DA equation is unchanged by the transformation y <--> -y, η <--> -η. The reason is that at no time is the amplitude of the depth perturbations FRo sufficiently large to make the nondimensional total depth differ from 1 by an O(1) factor. Hence cyclones and anticyclones behave in a similar fashion, with north and south reversed.

4. COMPARISON WITH SHALLOW-WATER EQUATIONS

To test the regimes of validity of the QG and DA equation sets, we have compared some numerical solutions of (3.1) and (3.31) with those for the shallow-water equations (henceforth SWE) given in D&K.

The domain for both equations is a cyclic E-W channel with rigid boundaries N-S, of dimension 15 deformation radii in each direction, using the scales described by (2.26) onwards. Initial conditions were chosen to mimic experiments C3 and C4 of D&K at the end of the initial forcing period, using a central height perturbation -0.038H (C3) and -0.42H (C4), varying radially as a Gaussian with length scale 86 km (=2R).

The QG equation (3.1) was solved using a 32-wave spectral decomposition E-W and 31 grid points N-S, again mimicking D&K as closely as possible. A small Laplacian diffusion was added to counteract the weak instability induced by an Adams-Bashforth time integration. The DA equation (3.31) was solved on a 31 x 31 grid with cyclic boundaries in both directions (acceptable since the beta term does not appear explicitly), and no diffusion. Integrations were just under 4 nondimensional time units, i.e. for 100 days. The results are presented nondimensionally.

(a) The QG results

(1) Cyclone C3

Figs. 1 and 2 compare the SWE and QG height and potential vorticity contours for experiment C3. (Height and streamfunction, nondimensionally equivalent, will be used interchangeably in what follows.) The SWE height contours show the familiar quasi-linear Rossby wave dispersal pattern, with a trailing pattern of shorter waves to the east of the height minimum. The QG results reproduce this quite well, although the centre of mass moves westward at the long wave speed, while in the SWE model the centre of mass moves slower than the long wave speed and somewhat north (also see Figs 4 and 5). The result is a westward and southward shift of the QG height contours compared with the SWE contours. The potential vorticity field, which is a far better indicator both of dynamics and goodness of fit, is compared in figs 1b, 2b. Again, the QG potential vorticity is reproduced qualitatively well, with similar regions of closed contours and surrounding wave fields, but it is consistently a little weaker (by one contour interval) than the SWE results, partly due to the explicit diffusion in the QG model.

Figs. 4 and 5 compare the paths of the height minima and potential vorticity maxima as functions of time between the SWE and QG for experiment C3. The more rapid westward movement of the QG system is visible both for the h and (less so) for the q extrema, as is the weaker northward movement of these in the QG simulation (0.5 to 0.75 deformation radii, compared with about 1 for the SWE).

Figs. 7 and 8 compare the amplitude of the h and q extrema in the two cases, over the 100 day integration. The SWE q is conserved almost exactly, whereas the QG version decays by 28% over the same period. Both

systems show a decay in the height extremum (by 23% in the SWE, and 32% for the QG version).

The QG system thus gives a reasonable qualitative prediction of the behaviour of the SWE system for the C3 experiment, but the quantitative results are in error.

(ii) Cyclone C4

We now consider the nonlinear C4 results. Figs. 10 and 11 compare SWE and QG h and q contours at a time of 100 days. Here two versions of potential vorticity are shown for the QG results:

$$\text{approximate } q = (\nabla^2\Psi + \beta y - \Psi/R^2)/f_o \qquad (4.1)$$

$$\text{real } q = (\nabla^2\Psi + \beta y - \Psi/R^2)/f_o\,(1+\Psi/R^2 f_o). \qquad (4.2)$$

The former is relevant to the QG theory, and the latter, from definition (2.24), includes the vortex stretching term, although formally this effect is small under QG assumptions. (In C3, the two versions for q were indeed almost identical.) The QG eddy again propagates westwards rather faster than the SWE eddy, and moves hardly northwards at all. There is evidence of a trailing Rossby wave behind the QG eddy, which is not visible in the SWE results. The approximate q field is 30% weaker than the real q field; the vortex stretching term is quite important in this cyclonic flow. However, even the 'real' q underestimates the SWE q by 25%. Neither q field conveys the degree of 'winding up' of q contours found in the SWE

case, although the diffusion present (50 m^2s^{-1}) would be sufficient to smooth the SWE result somewhat, as seen in D&K.

The (almost coincident) paths of the height and q extrema for this case are shown in Figs. 13 and 14. The QG path again moves too far west, (by almost a deformation radius) and insufficiently far north (by half a deformation radius), compared with the SWE path. The values of the extrema are shown in Figs. 16 and 17; in the SWE case the magnitudes of the extrema are fairly constant over time, but the QG case shows decay over the 100 day period of 10% (h) or 18% ('real' q).

Thus QG gives a qualitatively good picture of the pattern of the C4 eddy, but erroneous results for trajectory and strength.

(b) The DA (dispersal advection) results

(i) Cyclone C3

Figs. 1 and 3 compare the SWE and DA models for experiment C3. Again, two versions of the DA potential vorticity are shown:

$$\text{approximate } q = \beta y/f_0 - h/H \qquad (4.3)$$

$$\text{real } q = (v_x - u_y + f)H/f_0(H+h) \qquad (4.4)$$

where the former is the relevant quantity for the DA theory. Recall that the coordinate system in DA drifts westward at the long Rossby wave

speed. The h contours have a qualitatively reasonable shape, but are distinctly too weak compared with the SWE. The resulting q field is also far too weak: the DA contours after 100 days show a quasi-linear perturbation on the background q field, with all trace of a maximum lost.

Figs. 4 and 6 compare the paths of the extrema. The agreement between DA and SWE is very poor, and the q maximum disappears rapidly. Figs. 7 and 9 show the magnitude of the extrema over the 100 day period. The DA q's cannot be traced beyond 60 days, while the h minimum decays rapidly (by 55%, compared with only 28% in the SWE system).

Thus the DA system is a poor representation of the SWE for the C3 simulation. The poor fit is surprising, given the excellent parametric agreement.

However, the C4 simulation by the DA system is much more accurate (despite being beyond the DA parameter range $Ro \sim \epsilon^{3/2}$). Figs. 10 and 12 compare the h and q contours for this case. The shape and position of the h minimum and q maxima (after allowing for the coordinate drift) is excellent. The 'real' q contours successfully convey (with about the same degree of fragmentation) the winding-up of vorticity around the central core of the eddy (although no trace of this remains for the approximate DA q contours, which merely retain a central contour).

Figs. 13 and 15 show the paths traced by the h and q extrema (they almost perfectly overlie for this degree of nonlinearity). The DA extrema move a little further west than the SWE extrema (about 0.75 deformation

radii) and successfully capture the northward movement of the extrema (about 1.1 radii). The magnitudes of the extrema are also well caught: Figs. 16 and 18 compare these. Ignoring the approximate q (which is far too weak), h and q are constant in both cases, although the DA form shows a 13% variation over the 100 day period, finally recapturing its original value.

Thus the DA system gives an excellent description of the SWE dynamics for the C4 case, but a very poor one for the C3 case, for which it is apparently more suited parametrically.

5. AD HOC MODELS FOR THE MOTION OF A MATERIAL EDDY

When potential vorticity q is conserved for all fluid elements, any region of closed q contours can be regarded as a material eddy: fluid inside such a region must remain inside unless the closed contours connect to open contours by some process. In this section simple ad hoc models are proposed which allow rapid calculation of approximate eddy evolution, and which offer some insight into the self-propelling nature of strong eddies.

In the numerical experiments reported by D&K, the shapes of the material eddies (meaning the closed q-contour regions) are almost circular, and fluid elements inside the eddies follow roughly circular paths relative to the eddy "centre". Fig. 19 shows trajectories of fluid elements in experiments (C3) and (C4) of D&K. The straightest trajectories correspond to elements very near the position of the q extremum within the eddy, whereas the looping trajectories are for elements also within the eddy but further from the q extremum. Accordingly we will assume that fluid elements inside or near the eddy have exactly circular paths relative to the eddy "centre". (This point is not necessarily the geometric centre of the eddy.) Fluid elements outside the eddy have more complicated trajectories, and these are largely neglected in the model.

Given the vorticity distribution at a particular time, the velocity at the eddy "centre" can be deduced. We assume that the eddy as a whole

translates with this velocity, which will in general vary as the vorticity pattern changes.

An assumption about eddy size is also needed. To avoid the complications of changing eddy shape we will only consider fluid elements within some radius a of the eddy "centre", and choose this radius such that the associated circle encloses the material eddy.

We assume motion is quasigeostrophic. A particularly simple model is described first to introduce the basic dynamics, followed by a more complex version.

BASIC MODEL

Fig. 20 shows typical potential vorticity maps for cyclonic eddies. Suppose such a potential vorticity pattern is approximated by

$$q = \begin{cases} q_0(r) & 0 < r < a \\ \epsilon y & \text{otherwise,} \end{cases} \qquad (5.1)$$

so the circularly symmetric pattern $q(r)$ centred on the point (X_0, Y_0) represents the material eddy. For a cyclone,

$$q(r) \geq q(a) = \epsilon(Y_0+a) \qquad (5.2)$$

gives the idealised potential vorticity distribution shown in Fig. 21. (Corresponding anticyclonic cases have the internal and external q patterns matching at the southern eddy boundary.) The eddy centre in this case is chosen to be the geometric centre at (X_0, Y_0) at time t_0.

As the eddy translates and rotates, a fluid element inside will move from

$$(x_0, y_0) = (X_0, Y_0) + r(\cos\theta_0, \sin\theta_0) \qquad (5.3a)$$

to

$$(x, y) = (X, Y) + r(\cos\theta, \sin\theta) \qquad (5.3b)$$

when following a circular path relative to the eddy centre, which has moved to (X,Y). The change in angular position is

$$\phi = \theta - \theta_0. \qquad (5.4)$$

The fluid element conserves its quasigeostrophic potential vorticity

$$q(r) = Ro\ Z + \epsilon y \qquad (5.5)$$

where

$$Z = \zeta - F\eta = \nabla^2\eta - F\eta \qquad (5.6)$$

is the intrinsic vorticity. Thus the intrinsic vorticity must change as the latitude of the fluid element changes.

Outside the eddy, the movement of fluid elements is disregarded so Z remains zero there.

Each fluid element of area dA can be regarded as a Helmholtz vortex of strength ZdA. An element at (x,y) induces a velocity at (X,Y) of

$$(u,v) = \frac{Z\,dA}{2\pi r^2}\ K_1(F^{1/2}r)F^{1/2}r(y-Y, X-x) \qquad (5.7)$$

where K is a modified Bessel function. (See Zabusky & McWilliams 1982, who use discrete vortices in a similar model.) Note that $F^{1/2}r$ represents distance in units of Rossby radii. It is convenient to define

$$s = F^{1/2}r\ , \quad b = F^{1/2}a \qquad (5.8)$$

As F->0 , $sK_1(s)$ -> 1 (see Fig. 22) and fluid elements behave like ordinary point vortices.

We further assume that fluid elements conserve their area. Equivalently, changes in surface displacement following an element are neglected. Then the net effect at the eddy centre is to induce a zonal velocity

$$\begin{aligned} u_0 &= (F^{1/2}/2\pi)\int_0^a K_1(F^{1/2}r)\int_0^{2\pi}(y-Y)Z\ d\theta dr \\ &= (F^{1/2}/2\pi Ro)\int_0^a rK_1(F^{1/2}r)\int_0^{2\pi}\sin\theta\ [q(r)-\epsilon y]\ d\theta\ dr \end{aligned} \qquad (5.9)$$

(using equ. (5.5) to replace Z). This simplifies to

$$u_0 = -\tfrac{1}{2}(\epsilon/FRo)[\ 2 - b^2 K_2(b)] \qquad (5.10a)$$

which is always negative. A similar calculation gives the meridional central velocity

$$v_0 = 0 \qquad (5.10b)$$

so in this simple model the eddy moves due westward. As b (eddy radius in Rossby radii) increases u approaches $-\epsilon/F\ Ro$ which is the non-dimensional long Rossby wave speed. For small eddies u -> $-\epsilon a^2/4Ro$ as $F^{1/2}a$ -> 0, so in this limit speed is independent of F and is sensitive to eddy size.

With our choice of non-dimensional variables the rate of change of the central longitude X is

$$dX/dt = F\ Ro\ u_0/\epsilon = -1 + b^2 K_2(b)/2. \qquad (5.11)$$

The dependence of dX/dt on b is shown in more detail in Fig. 22. Both cyclones and anticyclones have the same speed for these quasigeostrophic eddies.

This prediction of dX/dt is reasonably good (see below), but the numerical experiments by D&K showed substantial meridional motion for small eddies which is not present in the above result.

IMPROVED MODEL

Suppose that the initial vorticity and surface displacement are circularly symmetric about the point (X_0, Y_0), so

$$\eta = \eta_0(r) \tag{5.12a}$$

$$\zeta = \zeta_0(r) = \nabla^2 \eta_0 \tag{5.12b}$$

with corresponding potential vorticity

$$q = q_0 = Ro\ Z_0(r) + \epsilon y \tag{5.12c}$$

Fig. 20 was constructed using such a pattern. For future reference we note that the meridional structure at $X = X_0$ can be written

$$q(X_0, y) = Ro\ Z_0(|y - Y_0|) + \epsilon(y - Y_0) + \epsilon Y_0 \tag{5.13}$$

Initially, motion due to this vorticity distribution is in circles centred on (X_0, Y_0), so we choose this to be the eddy centre. For a cyclone (anticyclone), this point is slightly equatorward (poleward) of the position where $|q|$ is largest inside the eddy (the eddy centre for the basic model).

The initial radius a of the model eddy is the distance from Y to the northern (for a cyclone) limit of the closed q contours: this boundary occurs where q_y vanishes and can be calculated from (5.13). The circular

model eddy thus encloses fluid outside the region of closed q contours, so in calculating eddy evolution the advection of some fluid around the eddy is taken into account.

Movement of the eddy centre is calculated as in the basic model. Conservation of potential vorticity requires

$$Z = Z_0(r) + \epsilon(y_0-y)/Ro \qquad (5.14)$$

which when substituted in (5.9) leads to

$$\begin{aligned} dX/dt &= -\tfrac{1}{2}\int_0^b s^2 K_1(s)(1-\cos\phi)ds \\ &= -1 + \tfrac{1}{2}b^2 K_2(b) + \tfrac{1}{2}\int_0^b s^2 K_2(s)\cos\phi \, ds \end{aligned} \qquad (5.15a)$$

where ϕ is angular displacement as defined by (5.4). The integral term modifies the estimate (5.10a) obtained from the basic model. The meridional motion is similarly found to be

$$dY/dt = \tfrac{1}{2}\int_0^b s^2 K_1(s) \sin\phi \, ds \qquad (5.15b)$$

It is useful at this stage to regard this model as a set of nested, rigid rings with angular displacements $\phi(r)$. As the rings rotate the potential vorticity of each element is unchanged, so its intrinsic vorticity must change with latitude, thus inducing a changing velocity at

the centre of the structure.

Initially $\phi = 0$ so $dX/dt = dY/dt = 0$. For a cyclone anticlockwise motion increases ϕ thus causing north-westward movement, whereas for an anticyclone ϕ decreases and motion is south-westward, in qualitative agreement with the shallow-water model results in D&K.

Quantitative calculations require some means of determining ϕ and b. To find ϕ, consider a ring of radius r with

$$\zeta - F\eta = \zeta_0(r) - F\eta_0(r) + \epsilon(y_0-y)/Ro \qquad (5.16)$$

Averaging around the ring (denoted by an overbar) gives

$$\bar{\zeta}(r) - F\bar{\eta}(r) = \zeta_0(r) - F\eta_0(r) + \epsilon(Y_0 - Y) \qquad (5.17)$$

In line with the earlier assumption that η is unchanged, we use $\bar{\eta}(r) = \bar{\eta}_0(r)$, so

$$(1/r)d(rV)/dr = (1/r)d(rV_0)/dr + \epsilon(Y_0 - Y)/Ro \qquad (5.18)$$

where

$$V = (\epsilon/Ro\ F)\ r\ d\phi/dt \qquad (5.19)$$

is the azimuthal velocity with initial value V_0. Integrating, we obtain

$$d\phi/dt = (Ro\ F/\epsilon)\ V_0/r + \tfrac{1}{2} F(Y_0-Y) \qquad (5.20)$$

In deriving (14) we assumed that $\phi = \phi(r)$, and in line with the above derivation of its rate of change, ϕ should be interpreted as the average rotation of a ring, which further ties in with the concept of nested rigid rings.

To complete the model, the eddy size must be altered as the eddy moves meridionally. The D&K experiments showed that as a cyclone moves north into a region of larger ambient q some small-scale processes mix the northern edge of the eddy with its surroundings. (This region is a prime candidate for instability due to the reversal of the q gradient there, steepened by the advance of the eddy.) Accordingly, one way of estimating the cyclone size is to require that q at the northern edge match an unchanged ambient value.

Mathematically, along a section through the eddy centre X we maintain the original profile outside the eddy,

$$q_{OUT}(X,y) = Ro\ Z_0(|(X,y)-(X_0,Y_0)|) + \epsilon(y-Y_0) + \epsilon Y_0 \qquad (5.21a)$$

while inside the eddy the initial profile (5.13) is displaced a distance $Y-Y_0$ to give

$$q_{IN}(X,y) = Ro\ Z_0(|y-Y|) + \epsilon(y-Y) + \epsilon Y_0 \qquad (5.21b)$$

These must match at the point Y+a for a cyclone (at Y-a for an

anticyclone), as shown diagrammatically in Fig. 23. This matching imposes a limit on the meridional displacement of an eddy: it can move until the extreme q value inside the eddy matches the background value, at which point the material eddy no longer exists.

The eddy size can only decrease - we prevent the eddy "unmixing" by the condition

$$da/dt \leqslant 0 \qquad (5.22)$$

To illustrate the behaviour of this model, two cases will be considered.

CASE 1: SOLID-BODY ROTATION

The basic equations simplify when all "rings" rotate at the same rate, so we first describe a cyclone with

$$V_0 = r \qquad 0 < r < 1 \qquad (5.23)$$

initially. Geostrophically this corresponds to a paraboloidal surface displacement. Then

$$dX/dt = -\tfrac{1}{2} [\ 2 - b^2 K_2(b)\ ]\ (\ 1-\cos\phi\ ) \qquad (5.24a)$$

$$dY/dt = \tfrac{1}{2} [\ 2 - b^2 K_2(b)\ ] \sin\phi \qquad (5.24b)$$

$$d\phi/dt = Ro\ F/\epsilon + \tfrac{1}{2}F(Y_0 - Y) \qquad (5.24c)$$

From (5.24b,c),

$$d^2Y/dt^2 = -\tfrac{1}{4}F[\ 2 - b^2K_2(b)\ ]\ \sin\phi \qquad (5.25)$$

If b is held fixed at the initial value $F^{1/2}$ then (5.25) is equivalent to the unforced pendulum equation, to be solved with the initial conditions

$$\phi = 0\ ,\quad d\phi/dt = Ro\ F/\epsilon \quad \text{at } t=t_0. \qquad (5.26)$$

The solutions are well-known (see for example Jordan & Smith 1977 for a description). Angular displacement increases monotonically when

$$Ro\ F/\epsilon > 2 - b^2K_2(b) \qquad (5.27)$$

The eddy latitude Y increases and then decreases back to Y_0 periodically while X decreases monotonically. As Ro F/ϵ is increased the meridional displacement decreases, so qualitatively this simple case predicts that stronger eddies propagate more directly westward.

When the inequality in (5.27) is reversed then ϕ first increases to some value ϕ_{MAX}, then decreases to $-\phi_{MAX}$, repeating the cycle periodically. The sense of rotation actually reverses. If the size of this weak eddy is allowed to vary as described above however, then it vanishes before reversal occurs. (It is not worth describing details here.)

Qualitatively, weak cyclones travel north-westward to merge with surrounding fluid with the same potential vorticity.

For strong eddies, Y differs little from Y_0. If the term $Y_0 - Y$ is neglected in (5.24c) then ϕ increases linearly with time, and the trajectory of the eddy centre is a cycloid, as shown in Fig. 24 (cf. Nof, 1984, for an example of such a trajectory).

CASE 2: GAUSSIAN STRUCTURE

A more realistic model for comparison with the D&K shallow-water experiments has a Gaussian initial surface displacement

$$\eta_0 = \eta_{00} \exp(-r^2) \qquad (5.28a)$$

with

$$|\eta_{00}| = \sqrt{(e/2)} \qquad (5.28b)$$

to give unit maximum speed at $r = 2^{-1/2}$. The initial vorticity is

$$\zeta_0 = -4(1-r^2)\eta_0 \qquad (5.28c)$$

To simulate experiments C2 to C4 in D&K we use

$$F = 4$$
$$\epsilon = 0.024 \qquad (5.29)$$

$$Ro = \begin{cases} 0.004 & (C2) \\ 0.008 & (C3) \\ 0.09 & (C4) \end{cases}$$

This choice of parameters gives the same ratio of maximum speed to long wave speed as in D&K, and the same amplitude of surface displacement. The corresponding initial quasigeostrophic potential vorticity maps are shown in Fig. 20.

Eddy evolution was then determined by integrating (5.15a,b) and (5.20), with the constraints (5.21) and (5.22) on size. The integration is for t = 0 -> 10, which is the time for long waves to travel 20 Rossby radii (and is 270 days dimensionally). The results can be seen in Fig. 25. In each case the initial material eddy (region of closed q contours) is shown dashed, together with the circumscribing circle of the model eddy. The trajectory of the eddy "centre" is drawn, marked at equal time intervals, and the material and model eddy sizes are again indicated at the end of the integration.

The strongest eddy (C4) travels almost due west after a small initial northward displacement. The distance covered is about 15 Rossby radii westward and about 0.3R north. In the SWE experiment (C4) the eddy travelled the same distance west, but 2R north, so the meridional displacement has again been underestimated. The agreement with westward distance is fortuitous: using the SWE model an anticyclone (A4) of the same size travelled 21R westward and 2R southward in the same time. (The

difference between these SWE cyclones and anticyclones is principally due to the substantial depth perturbations, which tend to speed up anticyclones and slow down cyclones relative to quasigeostrophic models.)

The cyclone (C3) is ten times weaker than (C4). The ad hoc model predicts initial north-westward movement, curving to follow an almost westward path, with a substantial decrease in eddy radius (see Fig. 25b). After 10 units of time displacement is about 10R west, 1.5R north. By comparison, the SWE cyclone after the same time has moved 8R west, 4R north, following an almost linear trajectory. The equivalent SWE anticyclone (A3) moves 10R west and 4R south.

The ad hoc model has simulated the decrease in eddy speed with size, but again underestimates meridional movement. Soon after time t=10 the SWE eddies (C3) and (A3) merge with their surroundings, but the ad hoc eddies with slower north-south displacement survive much longer.

Cyclone (C2) has half the amplitude of (C3). The ad hoc model predicts a north-west path, followed by an abrupt switch to south-west movement (see Fig. 25c). This change is associated with a reversal in the sense of rotation of the model eddy. A more stringent criterion for eddy size is to strip off rings as they cease to rotate. If this criterion is applied then the ad hoc (C2) vanishes at time t=6.4. As described in D&K, the material eddy in SWE (C2) travels north-west, then west, and is strongly influenced by the surrounding field of Rossby waves which are neglected in the ad hoc model.

6. Discussion

The object of this paper was to explore alternative sets of equations to describe the motion of isolated eddies on a beta-plane, and in particular to see if the lengthy integration times required by the shallow-water equations could be circumvented.

The quasigeostrophic model, for eddies with O(1) Froude number, performed reasonably well, although qualitative agreement with the shallow-water equations was conspicuously lacking. A new equation set, the dispersal advection equation, performs very poorly for weak eddies (for which it is derived) but extremely well for strong eddies. Both models suffer because they are predicated on small deviations from flat isopycnal surfaces, so that cyclones and anticyclones cannot be distinguished.

An ad hoc model describing the movement of the eddy centre was also derived. This demonstrates well the self-propelling nature of isolated eddies, and agrees qualitatively with the shallow-water equations in that wider eddies travel faster, stronger eddies travel more directly westward, and cyclones (anticyclones) move poleward (equatorward) respectively. However, this model also underestimates meridional motion, probably because of the neglect of motion outside the eddy.

Thus almost all the qualitative behaviour of the shallow-water equations was reproduced somewhere within the three systems studied, but no set reproduced all the behaviour. Unfortunately, too, with the

exception of the ad hoc model, integration times were not noticeably shorter for the QG or DA set than for shallow-water equations, because in the former case the inversion of the Laplacian takes time, and in the latter case a short timestep is required to maintain the stability of the dispersive term.

We conclude, then, that the only fully satisfactory way to reproduce the behaviour of the primitive equations for eddies of intermediate strength ($U/\hat{c} \geqslant 1$) and size (a few Rossby radii) is to <u>use</u> the primitive equations.

References

Ball, F. K., 1963: Some general theorems concerning the finite motion of a shallow rotating liquid lying on a paraboloid. *J. Fluid Mech.*, 17, 240-256.

Davey, M. K., and P. D. Killworth, 1984: Isolated waves and eddies in a shallow water model. *J. Phys. Oceanogr.*, 14, 1047-1064.

Dugan, J. P., R. P. Mied, P. G. Mignery and A. F. Schultz, 1982: Compact, intrathermocline eddies in the Sargasso Sea. *J. Geophys. Res.*, 87, 385-393.

Flierl, G. R., D. Larichev, J. C. McWilliams and G. M. Reznik, 1980: The dynamics of baroclinic and barotropic solitary eddies. *Dyn. Atmos. Oceans*, 5, 1-41.

Gent, P.R., and J.C. McWilliams, 1983: Regimes of validity for balanced models. *Dyn. Atmos. Oceans*, 7, 167-183.

Gent, P.R., and J.C. McWilliams, 1984: Balanced models in isentropic coordinates and the shallow water equations. *Tellus*, 36, 166-171.

Jordan, D. W., and P. Smith, 1977: Nonlinear ordinary differential equations. Clarendon Press, 360pp.

Killworth, P. D., 1983: On the motion of isolated lenses on a beta-plane.

J. Phys. Oceanogr., 13, 368-376.

Matsuura, T., and T. Yamagata, 1982: On the evolution of nonlinear planetary eddies larger than the radius of deformation. *J. Phys. Oceanogr.*, 12, 440-456.

McDowell, S. E., and H. T. Rossby, 1978: Mediterranean Water: An intense mesoscale eddy off the Bahamas. *Science*, 202, 1085-1087.

McWilliams, J. C., and G. R. Flierl, 1979: On the evolution of isolated nonlinear vortices. *J. Phys. Oceanogr.*, 9, 1155-1182.

Mied, R. P., and G. L. Lindemann, 1979: The propagation and evolution of cyclonic Gulf Stream rings. *J. Phys. Oceanogr.*, 9, 1183-1206.

Nof, D., 1984: Oscillatory drift of deep cold eddies. *Deep-Sea Res.*, 31, 1395-1414.

Redekopp, L. G., 1977: On the theory of solitary Rossby waves. *J. Fluid Mech.*, 82, 725-745.

Shen, C. Y., 1981: On the dynamics of a solitary vortex. *Dyn. Atmos. Oceans*, 5, 239-267.

Williams, G. P., and T. Yamagata, 1984: Geostrophic regimes, intermediate solitary vortices and Jovian eddies. *J. Atmos. Sci*, 41, 453-478.

Zabusky, N. J., and J. C. McWilliams, 1982: A modulated point-vortex model for geostrophic, β-plane dynamics. *Phys. Fluids*, 25, 2175-2182.

FIGURE CAPTIONS

Fig. 1 Contours of (a) depth h (contour interval c.i. =.0076) and (b) potential vorticity q (c.i. = .0176) for the SWE system (experiment C3) after 100 days integration. Negative contours are dashed. Units are nondimensional throughout.

Fig. 2 Contours of (a) depth h (contour interval c.i. =.0076) and (b) potential vorticity q (c.i. = .0176) for the QG system (experiment C3) after 100 days integration. Negative contours are dashed.

Fig. 3 Contours of (a) depth h (contour interval c.i. =.0076) and (b) potential vorticity q (c.i. = .0176) for the DA system (experiment C3) after 100 days integration. Negative contours are dashed. The contours are relative to the frame moving westwards at the long Rossby wave speed.

Fig. 4 Paths of h minima and q maxima for experiment C3 for the SWE system. Crosses mark 10 day intervals. Units are deformation radii. Dashes show q, firm line h.

Fig. 5 Paths of h minima and q maxima for experiment C3 for the QG system. Crosses mark 10 day intervals. Units are deformation radii. Dashes show q, firm line h.

Fig. 6 Path of h minima for experiment C3 for the DA system.

Crosses mark 10 day intervals. Units are deformation radii. The predicted potential vorticity is difficult to follow, and is not shown.

Fig. 7 Values of the h minimum and q maximum over the 100 day period for experiment C3 for the SWE system. The full line shows -h, the dashed line q.

Fig. 8 Values of the h minimum and q maximum over the 100 day period for experiment C3 for the QG system. The full line shows -h, the dashed line q.

Fig. 9 Values of the h minimum and q maximum over the 100 day period for experiment C3 for the DA system. The full line shows -h, the dashed line the approximate q, and the dotted line the 'real' q.

Fig. 10 Contours of (a) depth h (contour interval c.i. =0.084) and (b) potential vorticity q (c.i. = 0.3) for the SWE system (experiment C4) after 100 days integration. Negative contours are dashed.

Fig. 11 Contours of (a) depth h (contour interval c.i. =0.084); (b) approximate potential vorticity q (c.i. = 0.3); and (c) real potential vorticity q (c.i. = 0.3) for the QG system (experiment C4) after 100 days integration. Negative contours are dashed.

Fig. 12 Contours of (a) depth h (contour interval c.i. =0.084); (b) approximate potential vorticity q (c.i. = 0.3); and (c) real potential vorticity q (c.i. = 0.3) for the DA system (experiment C4) after 100 days integration. Negative contours are dashed.

Fig. 13 Paths of h minima and q maxima for experiment C4 for the SWE system. Crosses mark 10 day intervals. Units are deformation radii. (Only one curve is shown, as the curves are almost coincident.)

Fig. 14 Paths of h minima and q maxima for experiment C4 for the QG system. Crosses mark 10 day intervals. Units are deformation radii. (Only one curve is shown, as the curves are almost coincident.)

Fig. 15 Paths of h minima and q maxima for experiment C4 for the DA system. Crosses mark 10 day intervals. Units are deformation radii. (Only one curve is shown, as the curves are almost coincident.) The contours are relative to the frame moving westwards at the long Rossby wave speed.

Fig. 16 Values of the h minimum and q maximum over the 100 day period for experiment C4 for the SWE system. The full line shows -h, the dashed line q.

Fig. 17 Values of the h minimum and q maximum over the 100 day period for experiment C4 for the QG system. The full line shows -h, the dashed line the approximate q, and the dotted line the 'real' q.

Fig. 18 Values of the h minimum and q maximum over the 100 day period for experiment C4 for the DA system. The full line shows -h, the dashed line the approximate q, and the dotted line the 'real' q.

Fig. 19 Trajectories of fluid elements from the shallow-water experiments described in D.& K. Distance units are Rossby radii. Forcing for day 0-->2π was centred on (0, 0).
(a) Cyclone (C4). The long trajectory covers 100 days, starting from the centre of the forced region. The short trajectory for day 0-->12 starts 0.25 Rossby radii south of the long one. The path of the material eddy, measured by the position of maximum potential vorticity, is very similar to the long trajectory.
(b) Cyclone (C3). Trajectories for day 0-->100. The material eddy closely follows the thick trajectory.

Fig. 20 Quasigeostrophic potential vorticity maps for a Gaussian surface displacement, with $F = 4$, $\epsilon = 0.024$. The unit of distance is $F^{1/2} = 2$ Rossby radii.
(a) Ro = 0.09 represents cyclone (C4).
(b) Ro = 0.008 represents cyclone (C3).

(c) Ro = 0.004 represents cyclone (C2).

Fig. 21 Idealised potential vorticity distribution for a cyclone for the basic ad hoc model. Inside the eddy $q = q_0(r)$, while $q = \epsilon y$ outside the eddy.

Fig. 22 (a) $1 - s^2K_2(s)/2$ gives the westward speed of an eddy of radius s (Rossby radii) as a fraction of the long Rossby wave speed.

(b) $s^2K_1(s)$ measures the influence of a ring of radius s (Rossby radii) on the motion of the eddy as a whole.

(c) $sK_1(s)$ measures the velocity induced by a Helmholtz vortex as a fraction of that induced by an ordinary point vortex at a distance of s Rossby radii.

Fig. 23 Meridional sections of potential vorticity for a cyclonic eddy with centre (X,Y) illustrating the ad hoc model matching. The dashed line represents the initial profile $q_0(X_0,y)$. This is displaced a distance $Y - Y_0$ within the model eddy, as shown by the thick line, and matches the unchanged ambient profile $q_0(X,y)$, shown by the thin line, at $y = Y+a$. Thus the model eddy radius a is determined.

Fig. 24 The cycloidal trajectory for a strong cyclonic eddy with uniform rotation, showing initial northward movement turning west, then southwest, then repeating for each eddy

revolution.

Fig. 25 Eddy evolution predicted by the improved ad hoc model. In each case the model eddy is initially centred on (0,0), with size indicated by a solid circle. The dashed circle represents the size of the material eddy. The distance unit is $F^{1/2}$ = 2 Rossby radii, with parameters F = 4 ,ϵ = 0.0024. In the time t = 0-->10 shown, a long Rossby wave would travel 10 units of distance westward.

(a) Ro = 0.09 represents cyclone (C4).

(b) Ro = 0.008 represents cyclone (C3).

(c) Ro = 0.004 represents cyclone (C2).

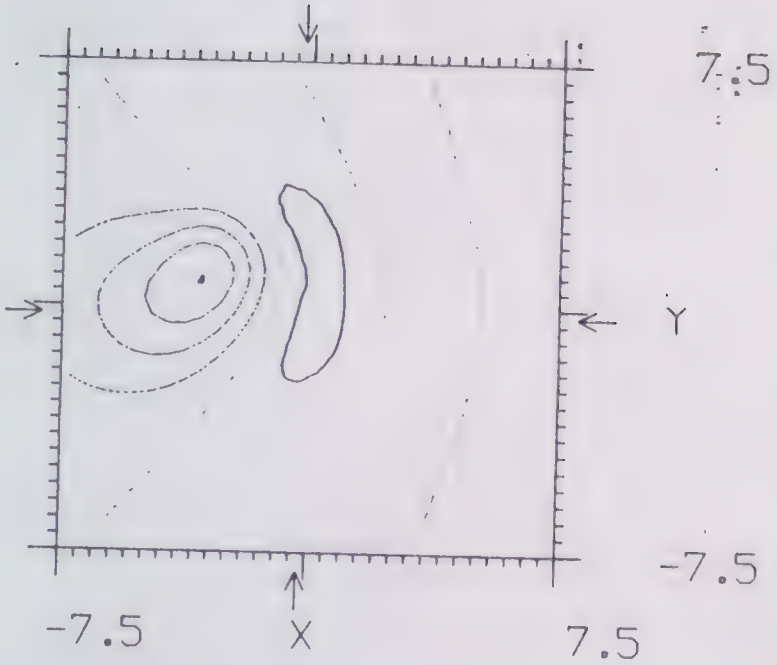

Fig. 1a

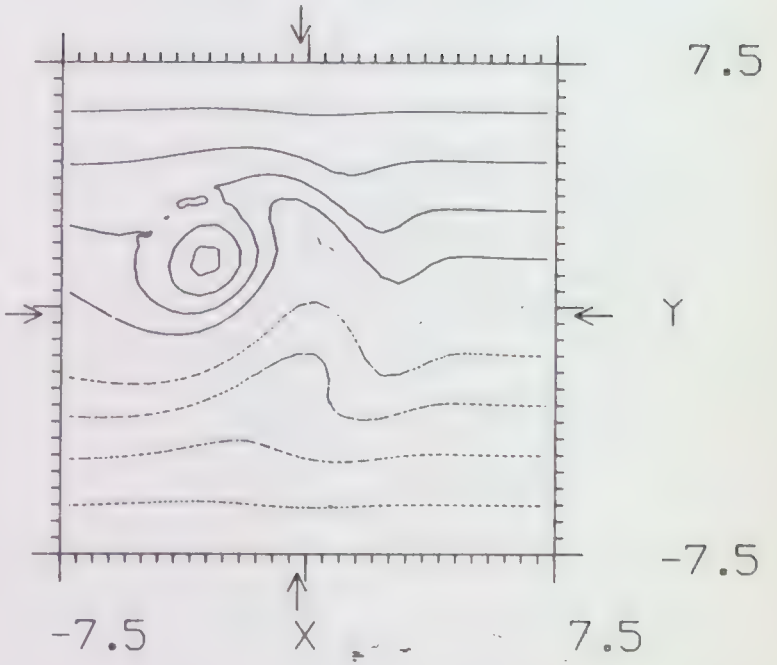

Fig. 1b

Fig 2b

Fig 2a

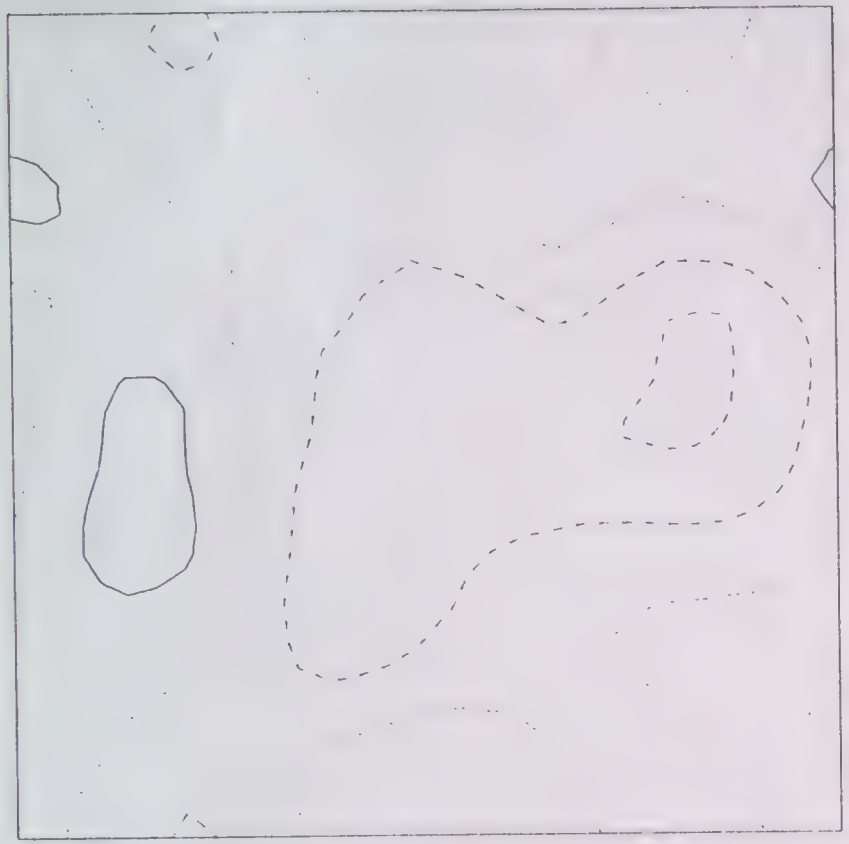

Fig 3a

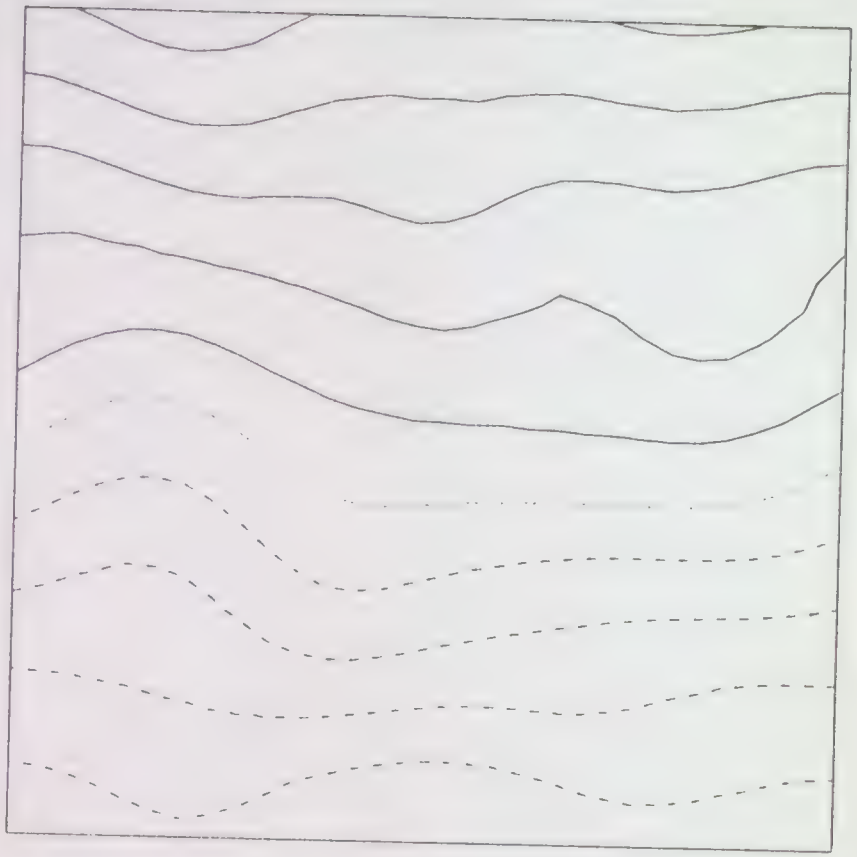

Fig 3b

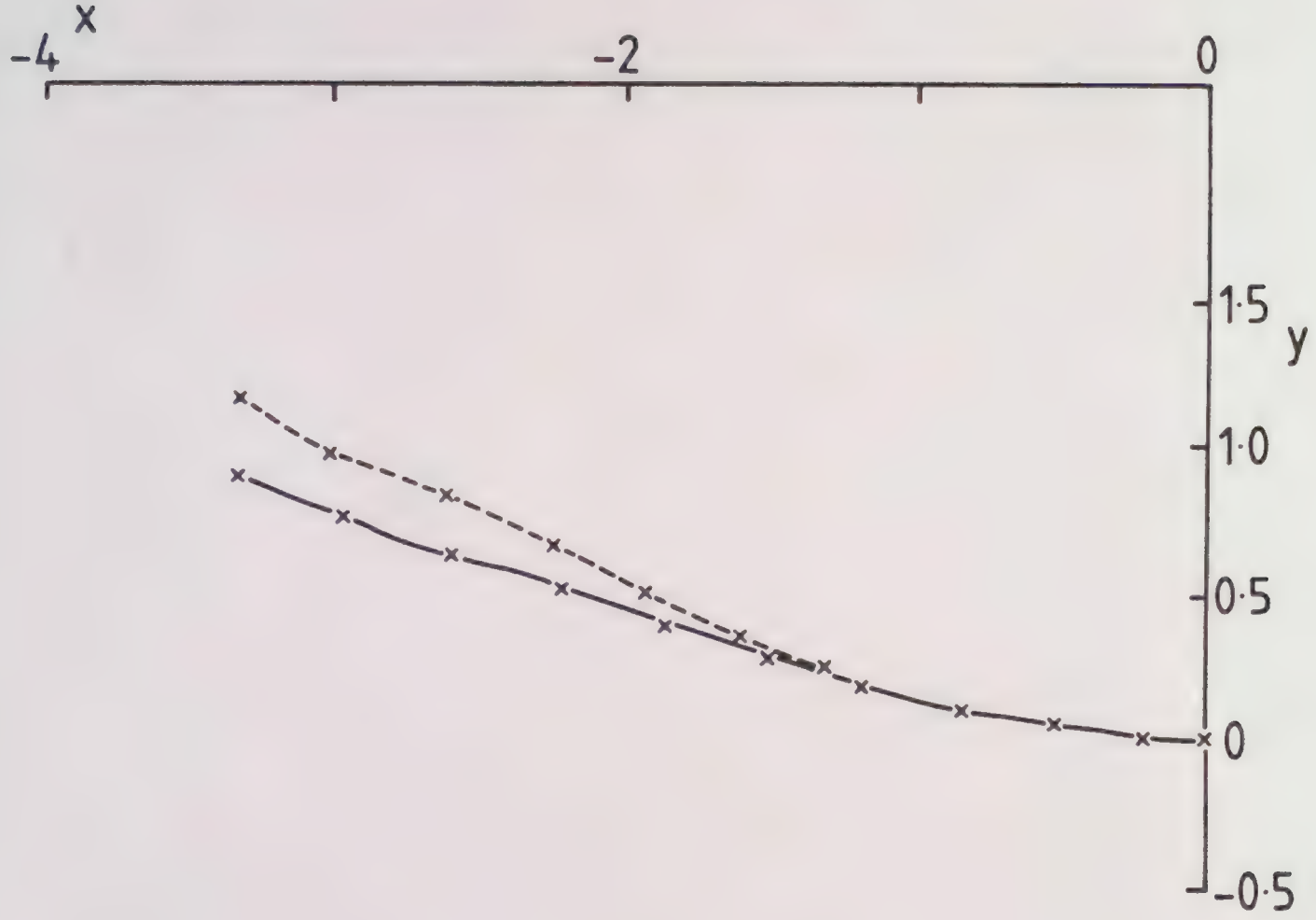

Fig. 4

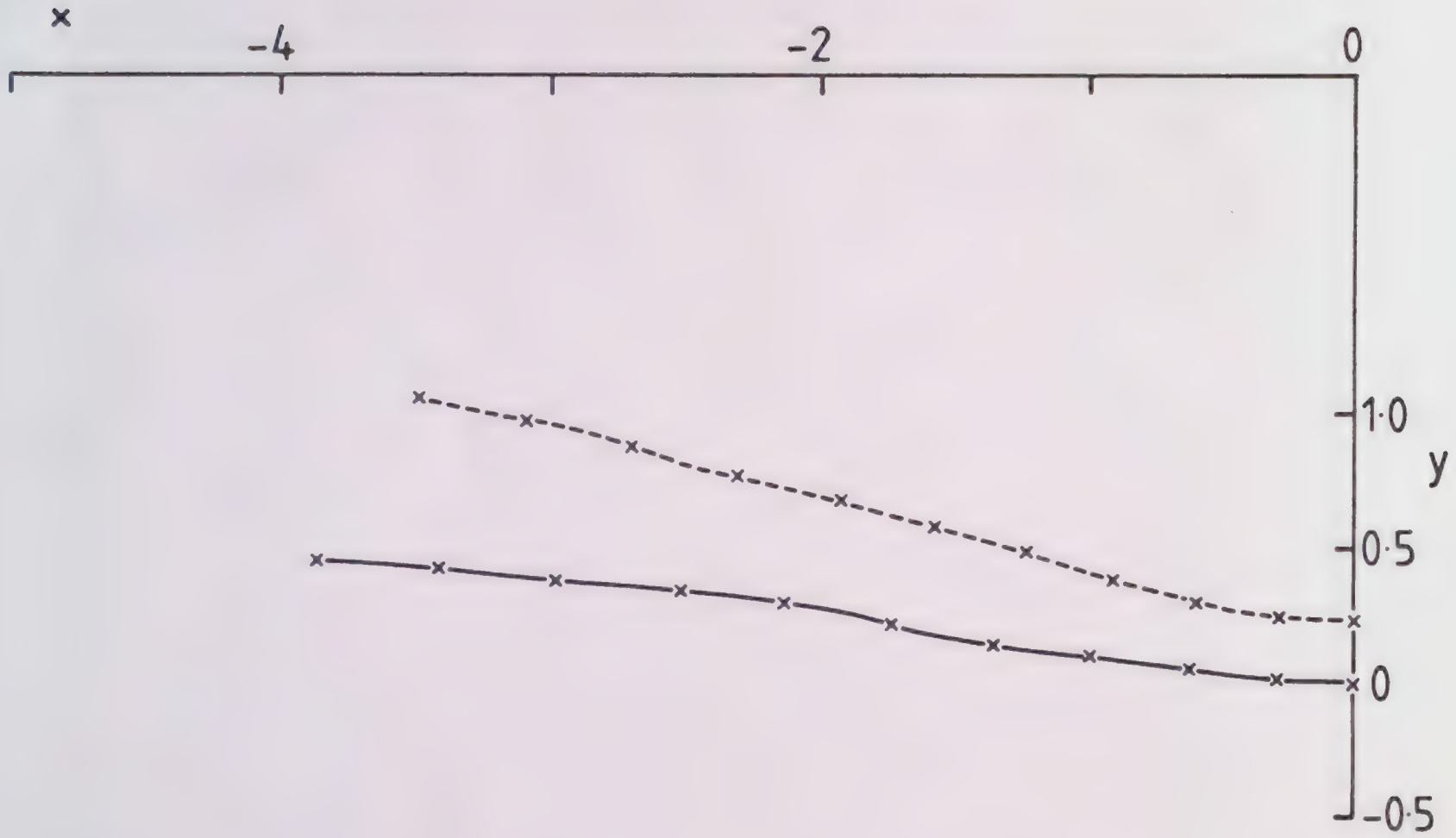

Fig. 5

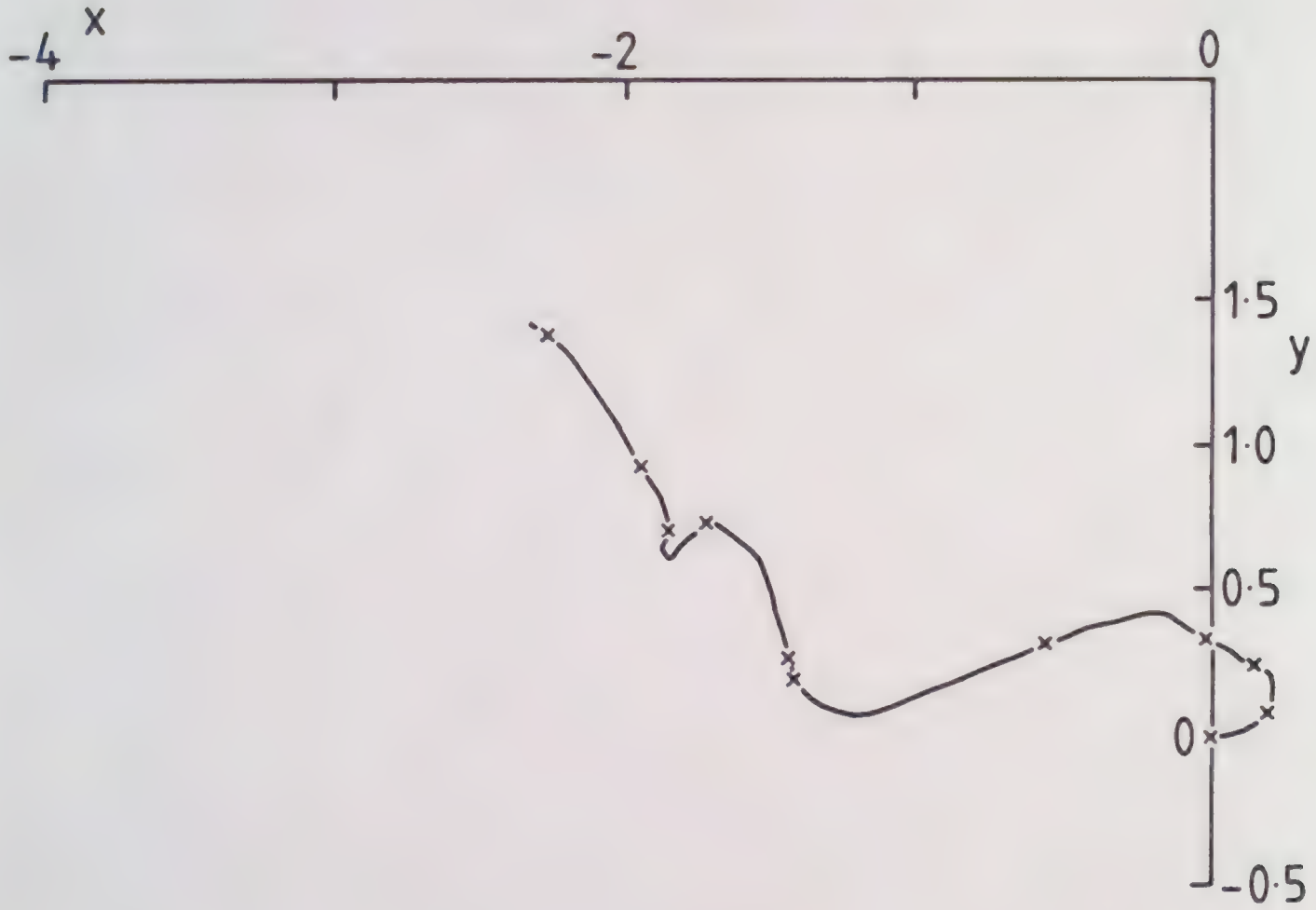

Fig. 6

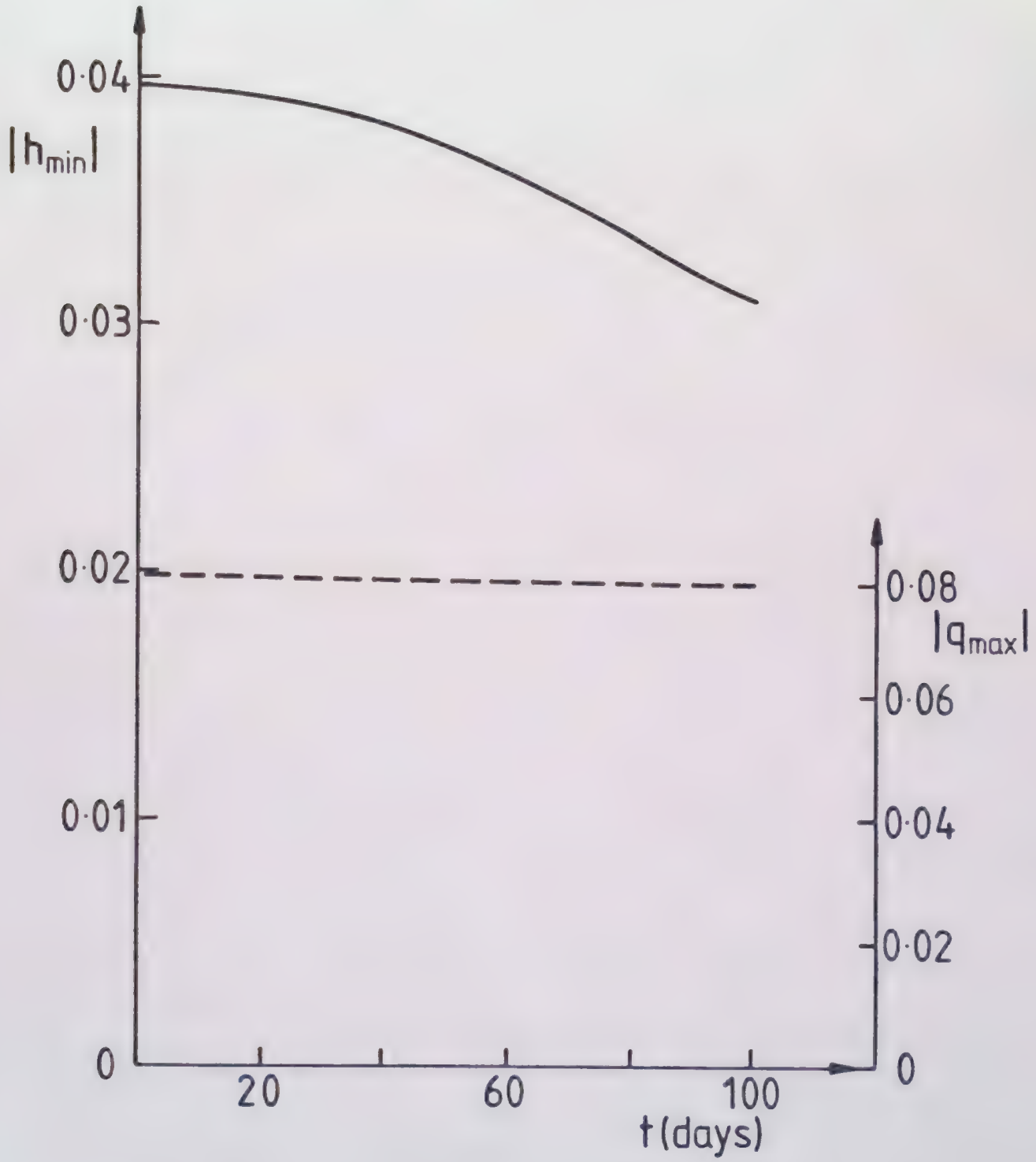

Fig. 7

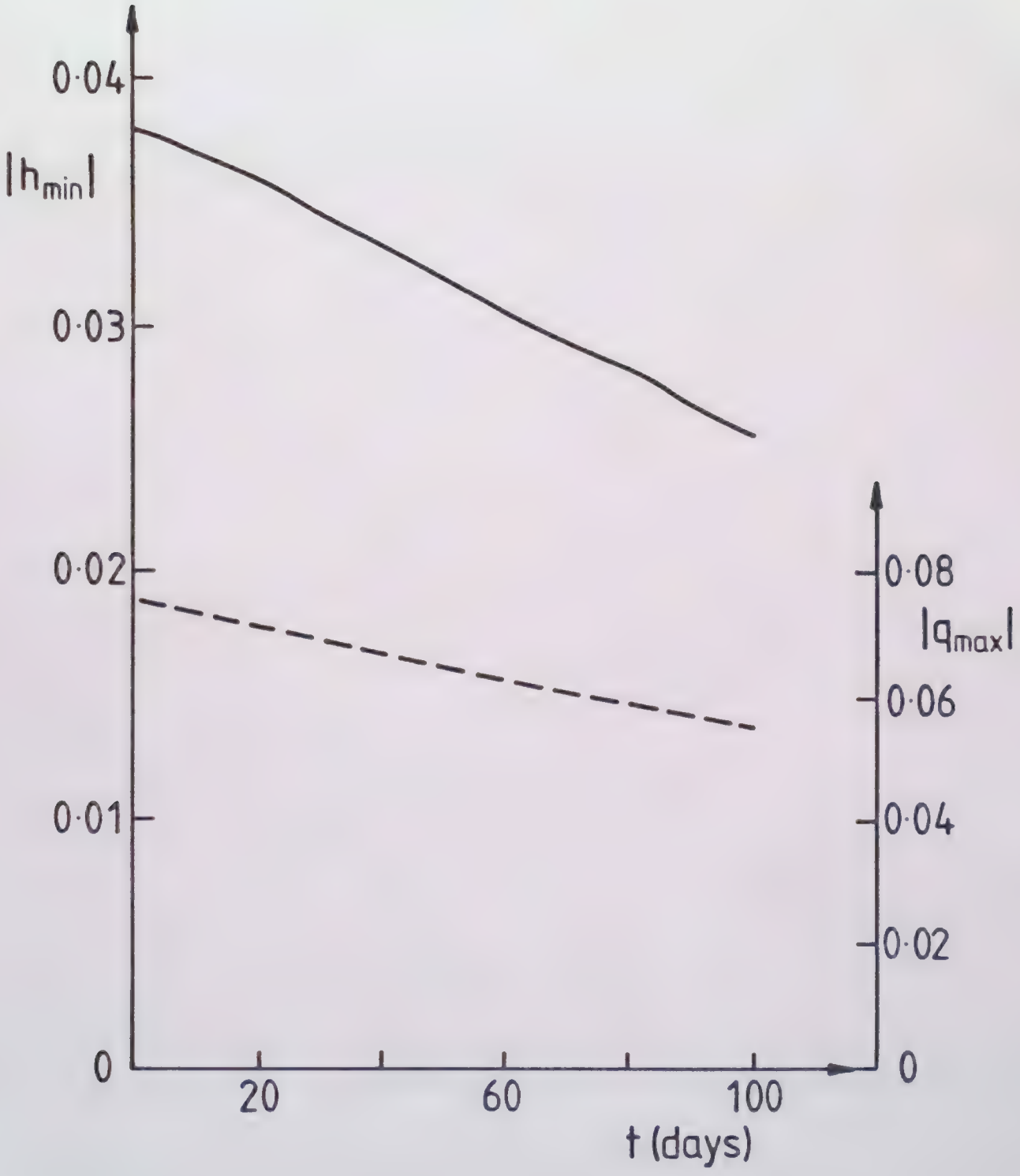

Fig. 8

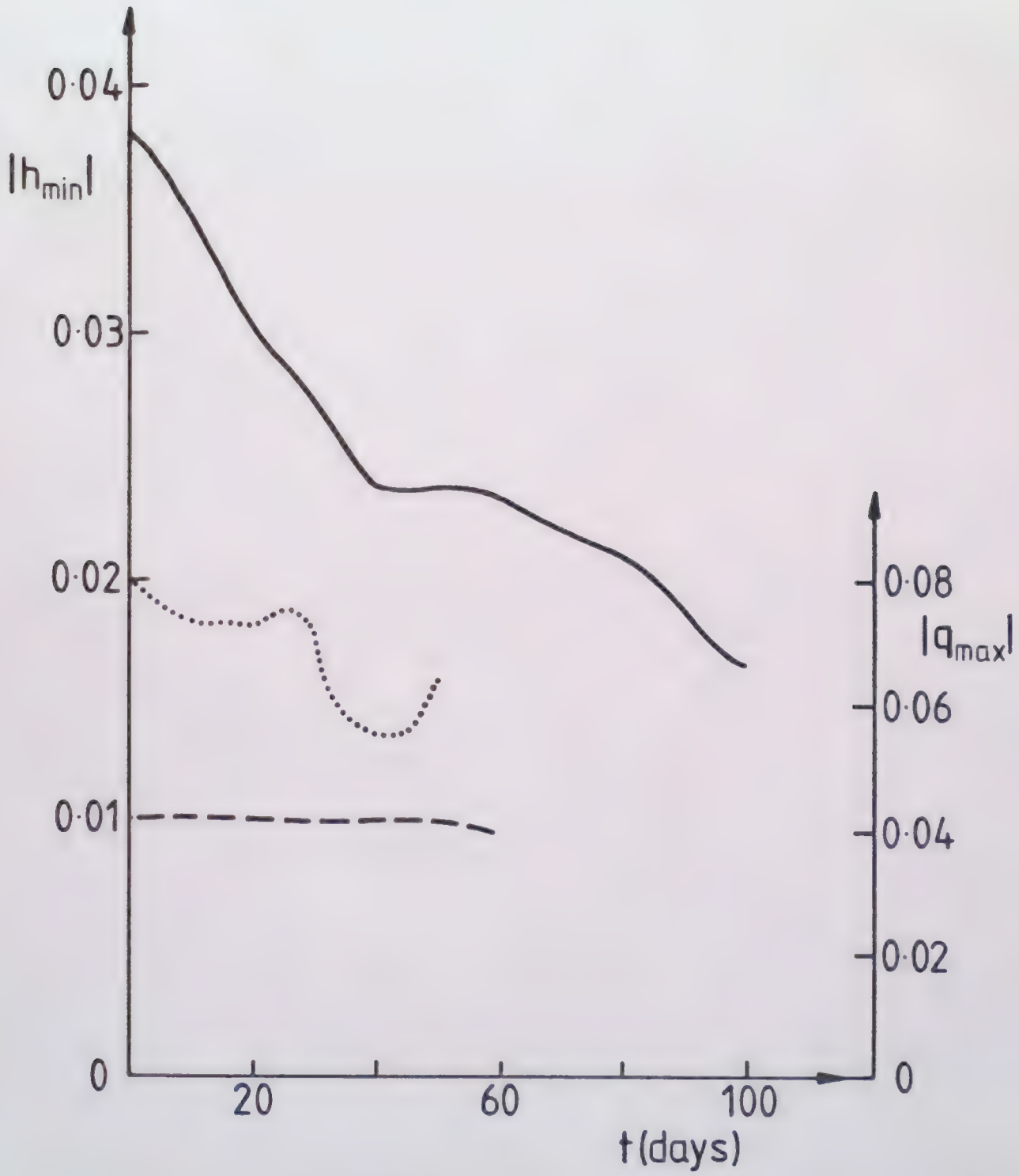

Fig. 9

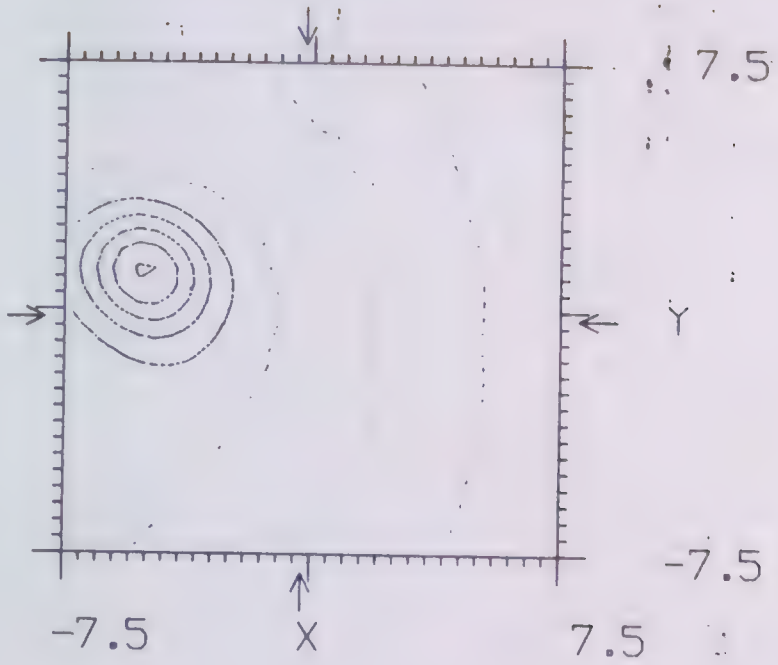

Fig. 10a

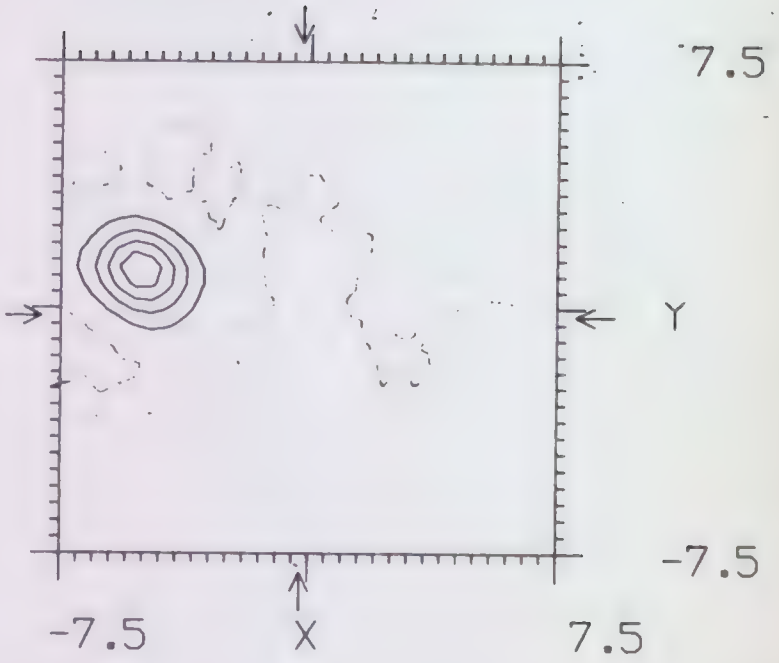

Fig. 10b

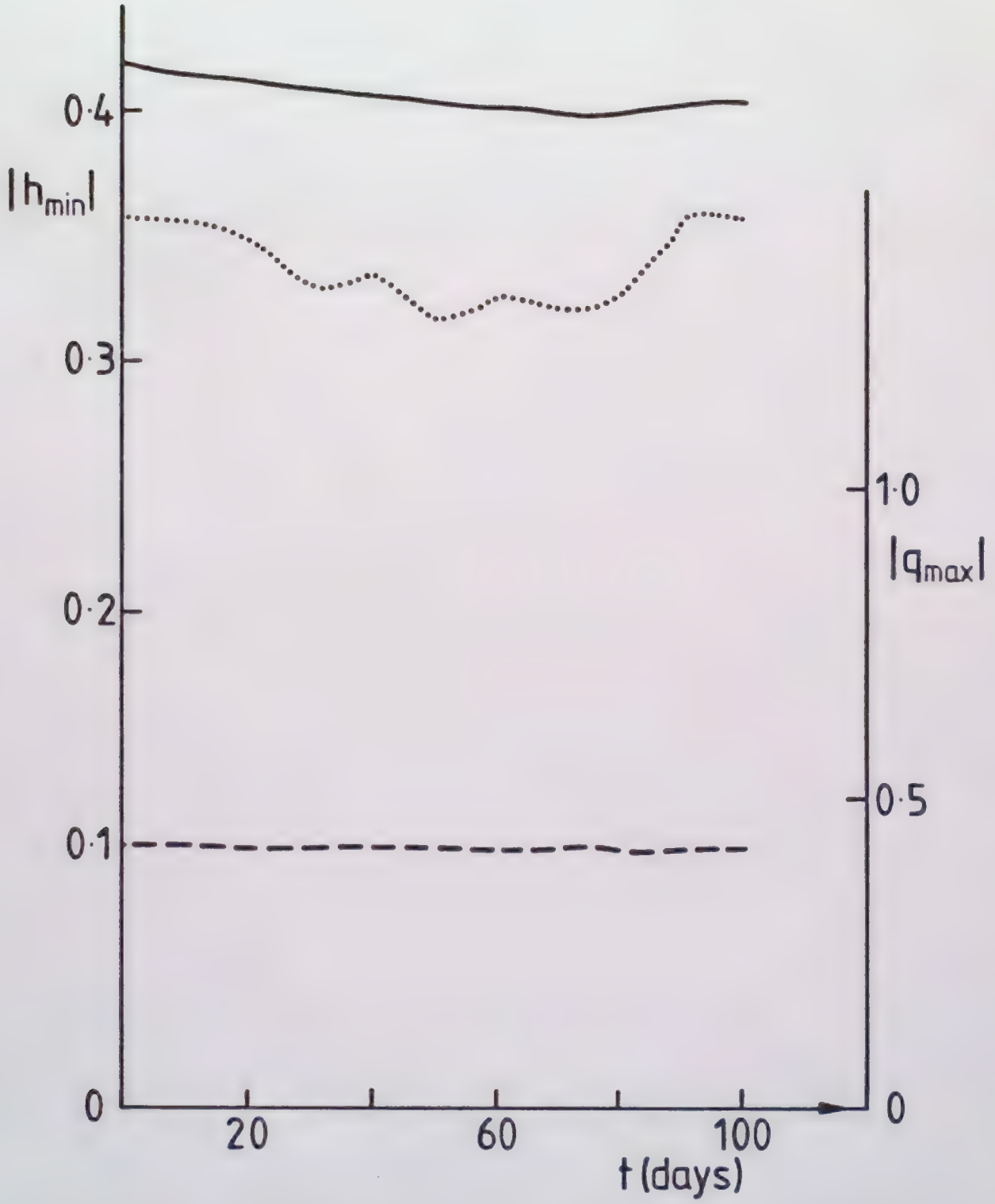

Fig. 18

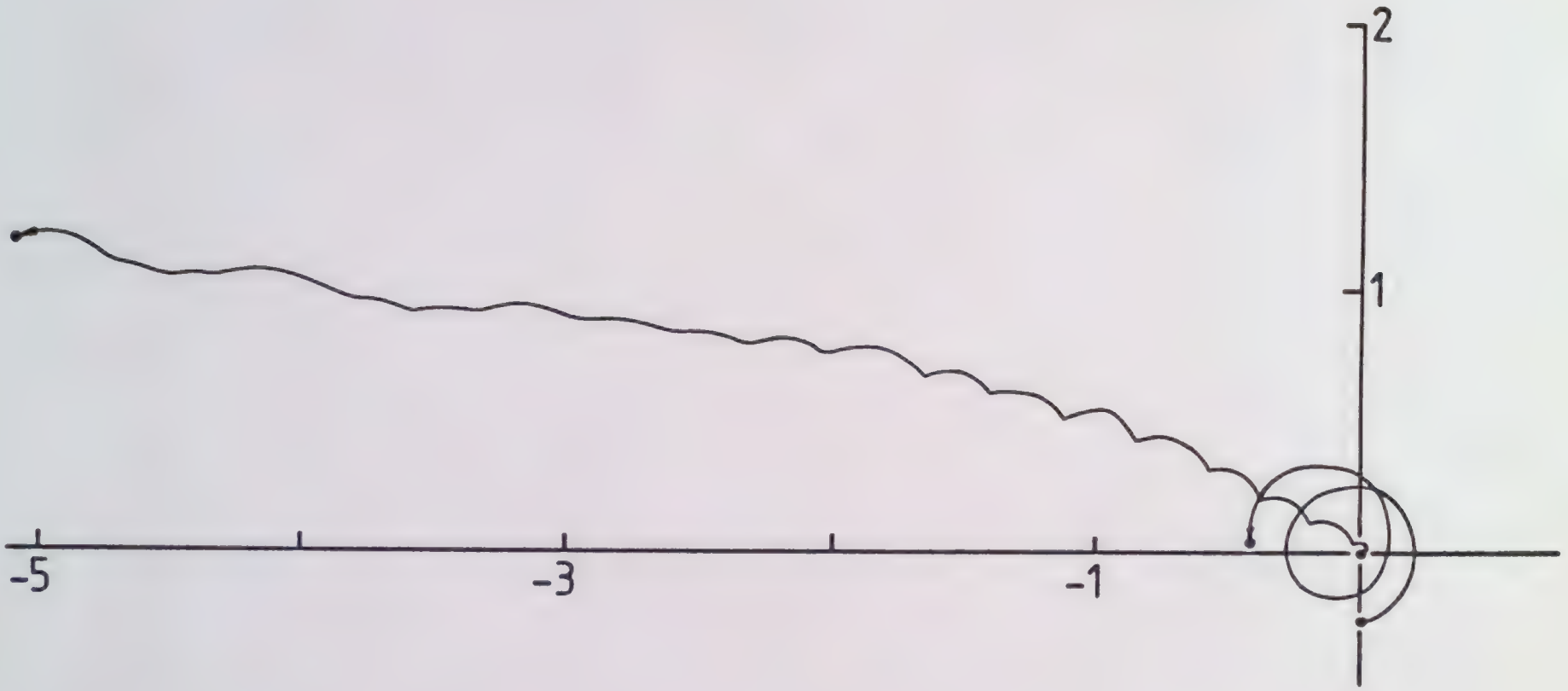

Fig. 19a

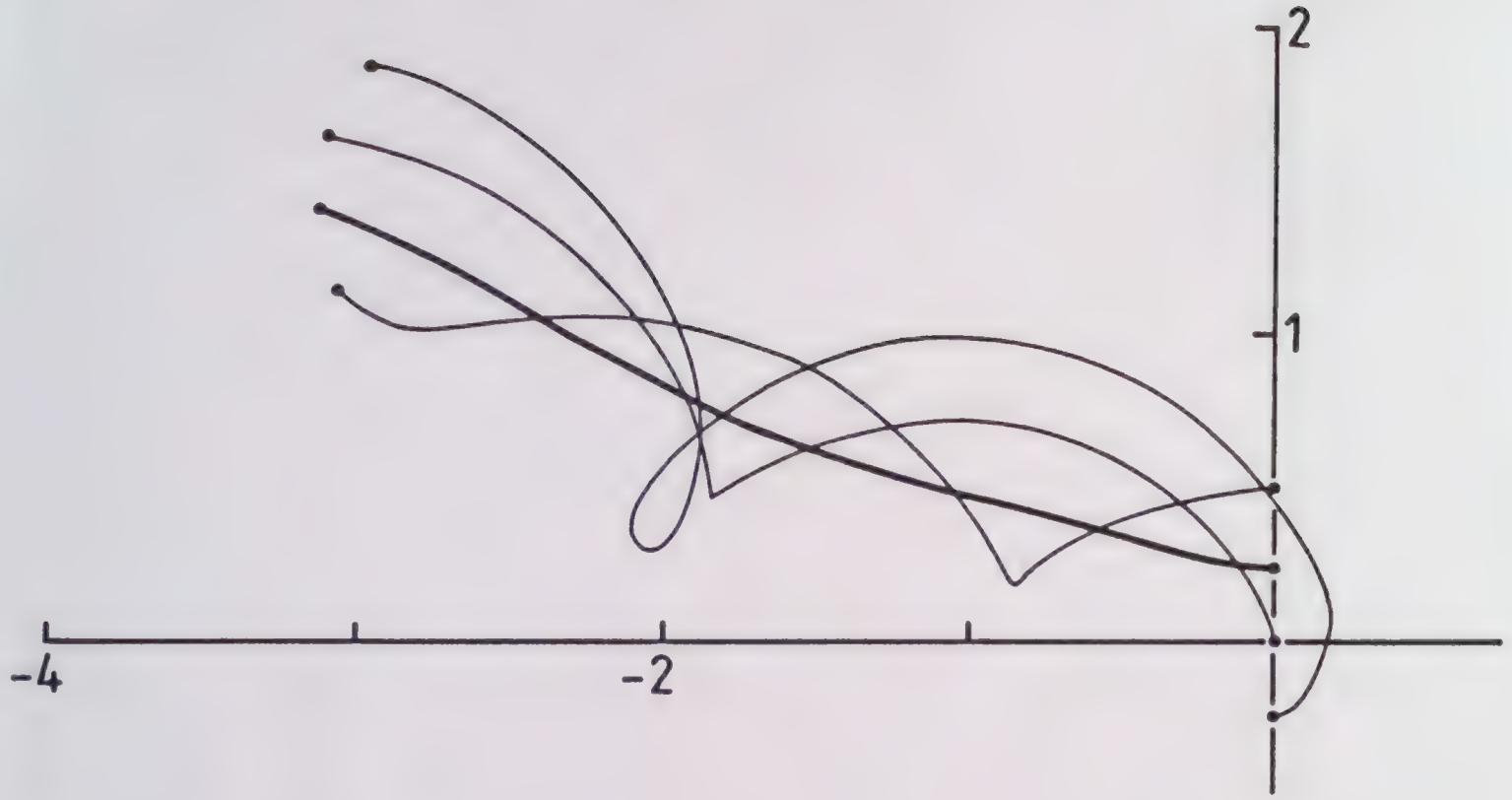

Fig. 19 b

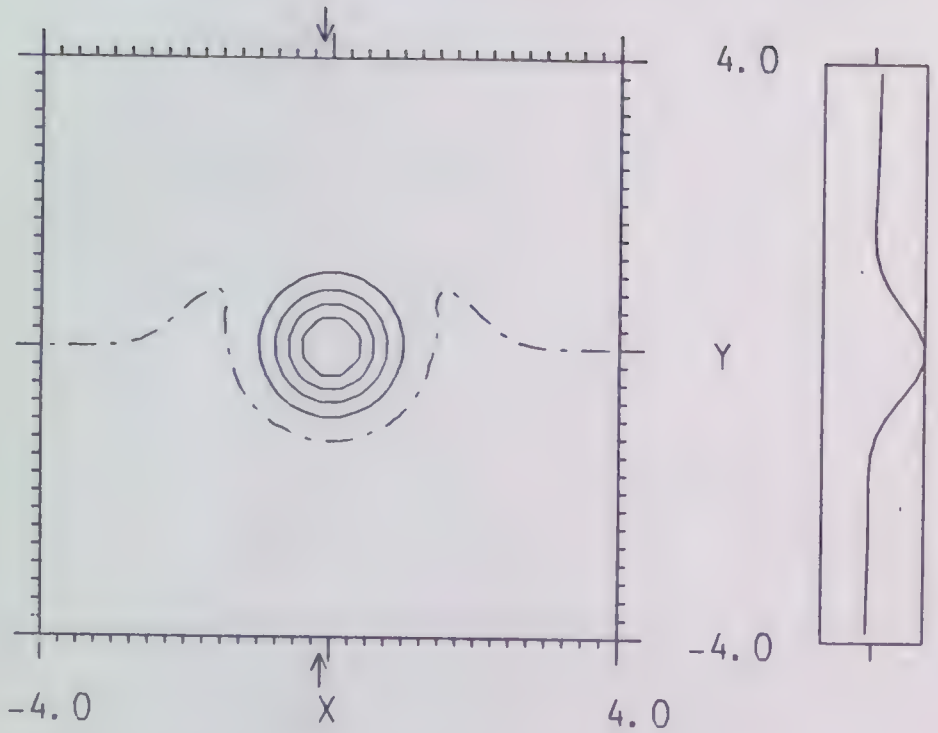

Fig. 20a

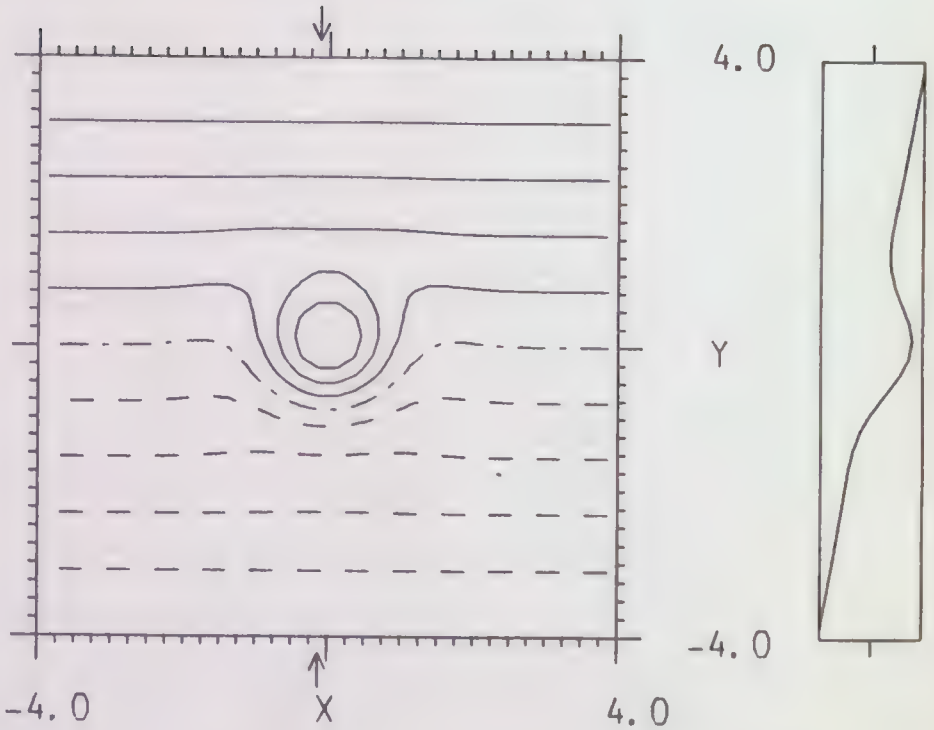

Fig. 20b

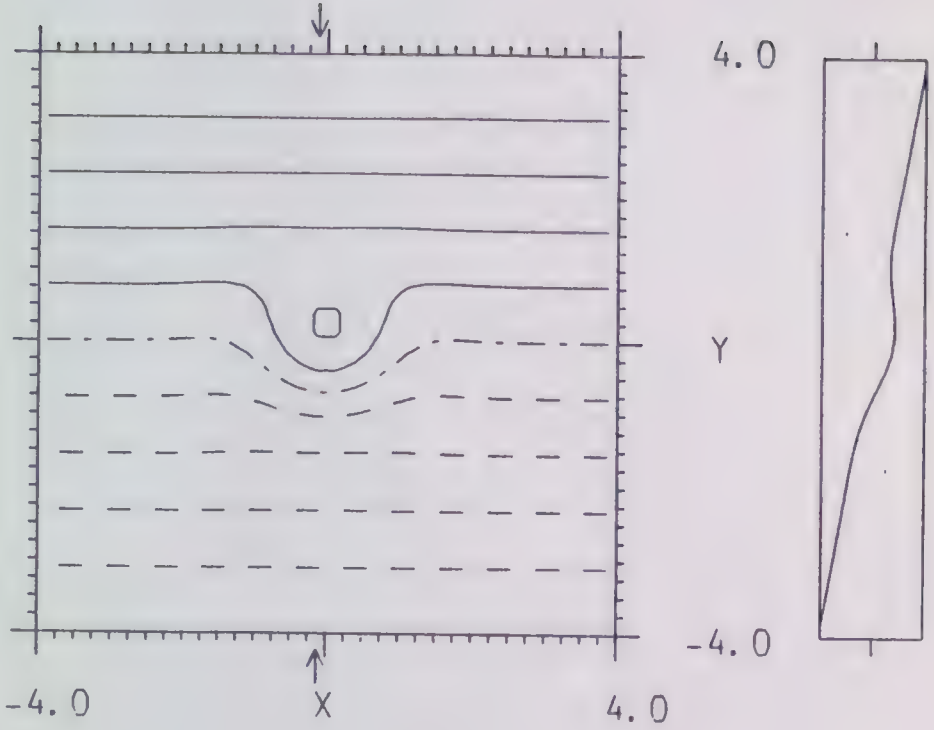

Fig. 20c

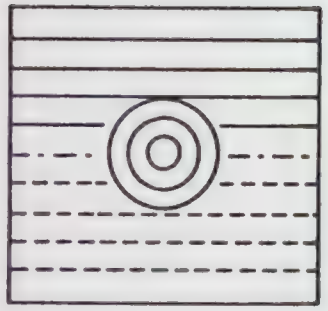

Fig. 21

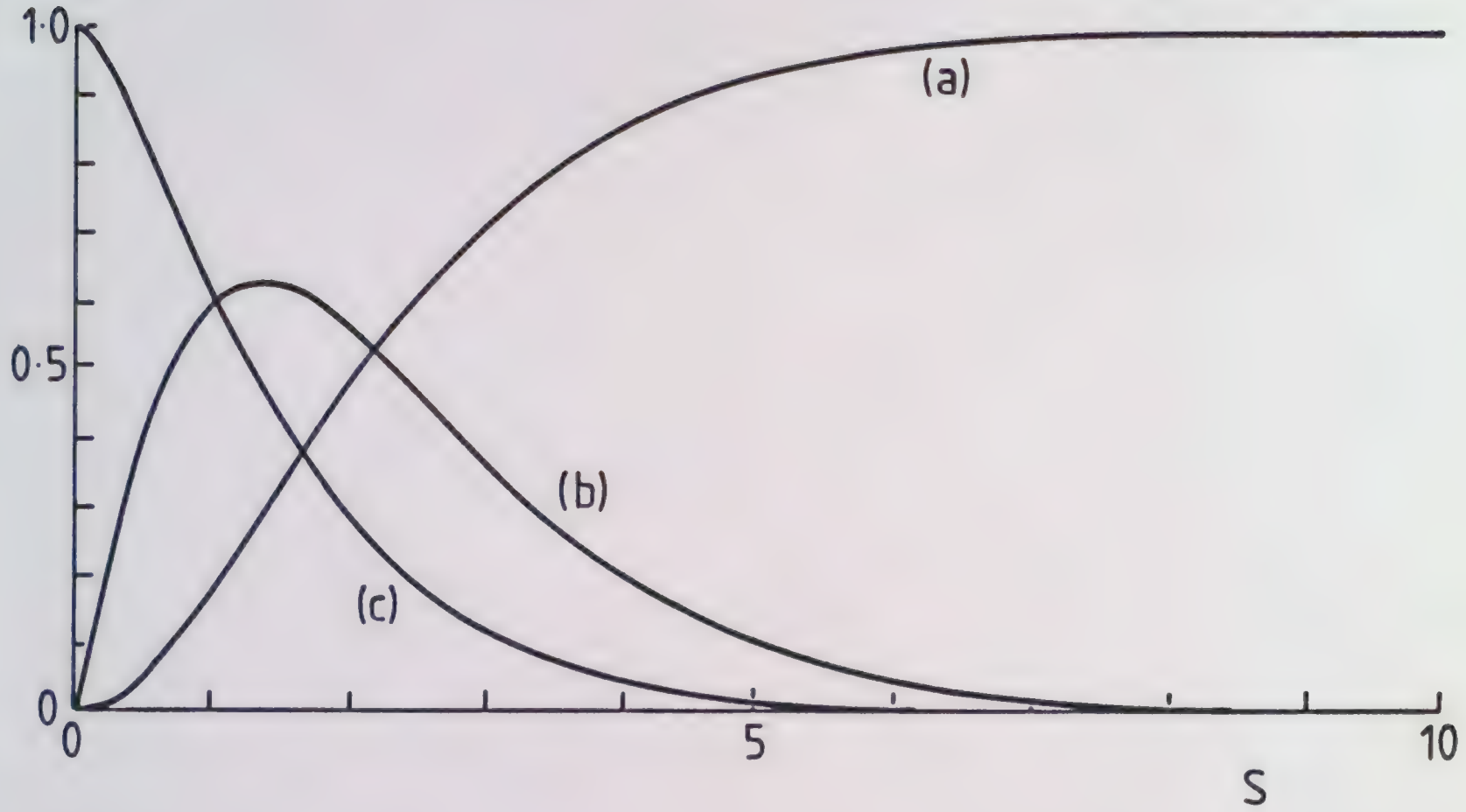

Fig. 22

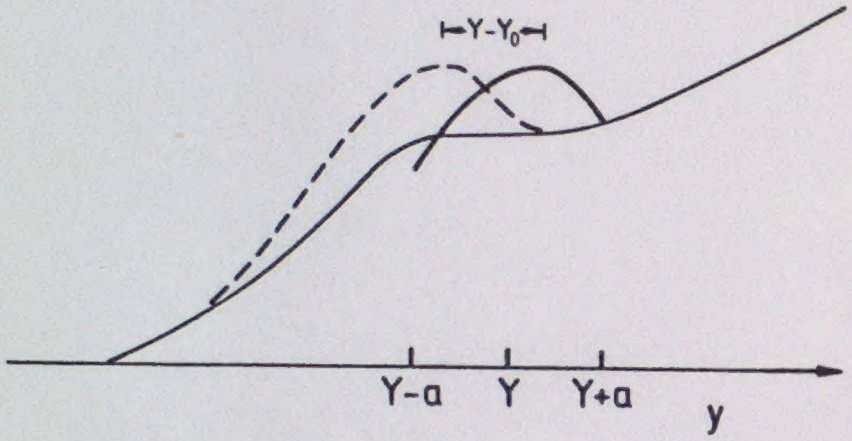

Fig. 23

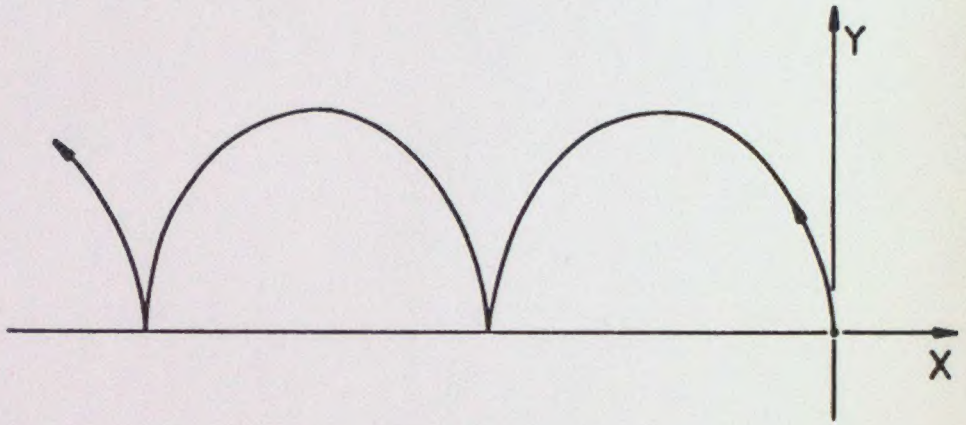

Fig. 24

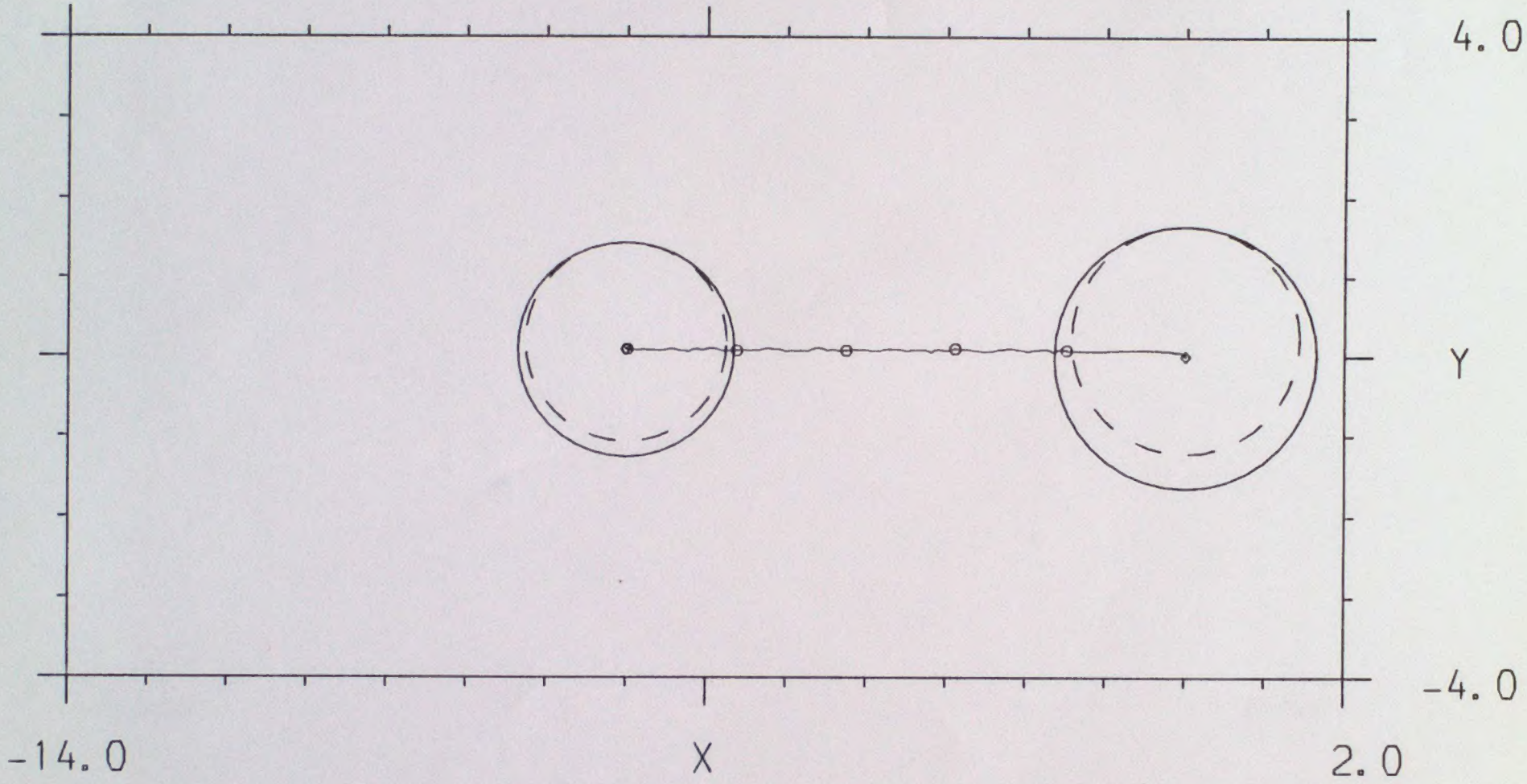

Fig. 25a

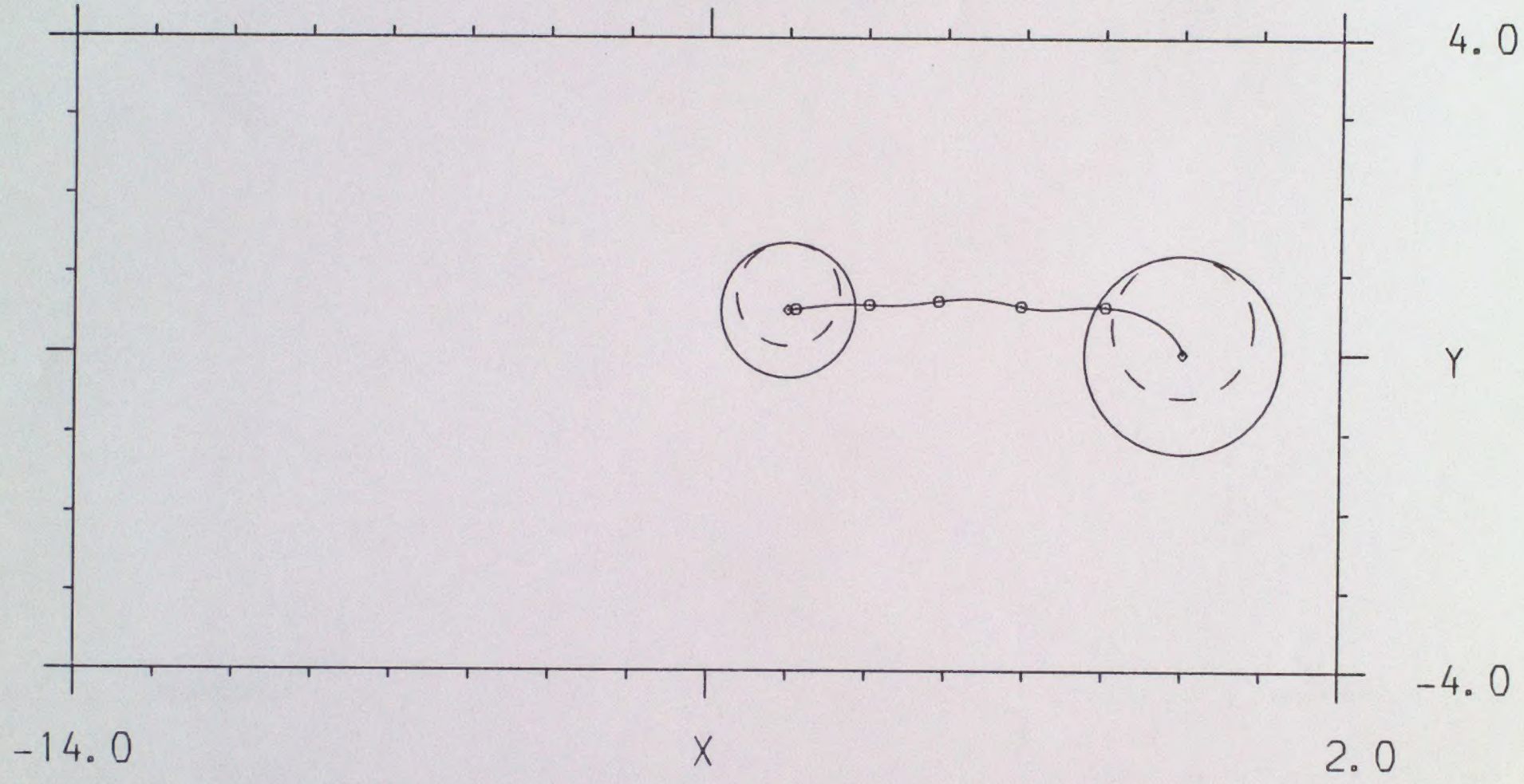

Fig. 25b

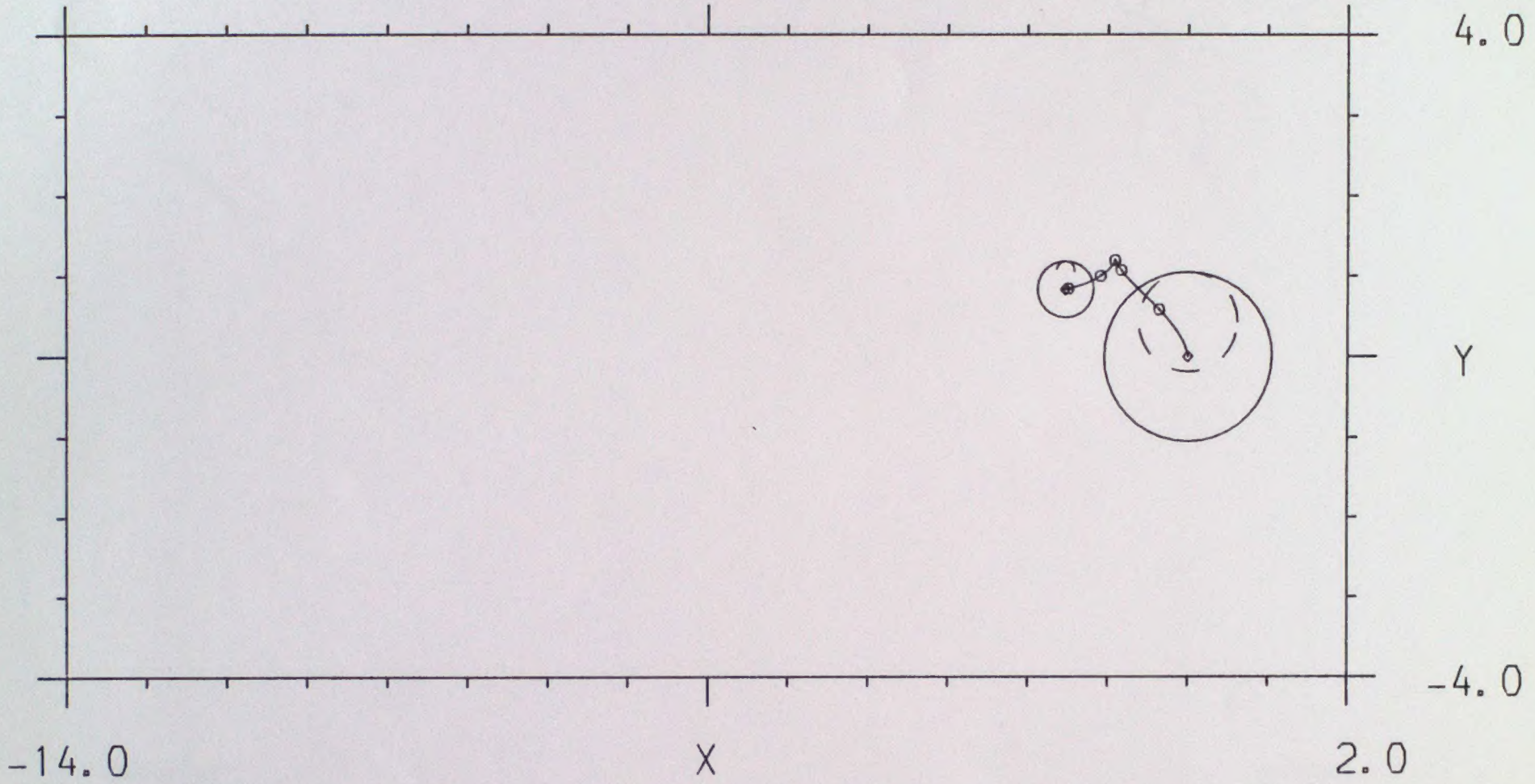

Fig. 25c